DEVELOPMENT OF AN AUTOMATED DEVICE FOR THE OPTIMIZED REGULATION OF CEREBROSPINAL FLUID (CSF)

by

Muhammad Waleed Anjum

A Thesis Submitted to the Faculty of

College of Engineering and Computer Science

In Partial Fulfillment of the Requirements for the Degree of

Master of Science

Florida Atlantic University

Boca Raton, FL

December 2023

DEVELOPMENT OF AN AUTOMATED DEVICE FOR OPTIMIZED

REGULATION OF CEREBROSPINAL FLUID (CSF)

by

Muhammad Waleed Anjum

This thesis was prepared under the direction of the candidate's thesis advisor, Dr. Waseem Asghar, Department of Electrical Engineering and Computer Science, and has been approved by all members of the supervisory committee. It was submitted to the faculty of the College of Engineering and Computer Science and was accepted in partial fulfillment of the requirements for the degree of Master of Science.

SUPERVISORY COMMITTEE:

Waseem Asghar, Ph.D.
Thesis Advisor

Imadeldin Mahgoub, Ph.D.

Mohammad Ilyas
Mohammad Ilyas (Nov 21, 2023 09:47 EST)
Mohammad Ilyas, Ph.D.

Hari Kalva
Hari Kalva (Nov 30, 2023 09:46 EST)
Hari Kalva, Ph.D.
Interim Chair, Department of Electrical Engineering and Computer Science

Stella N. Batalama, Ph.D.
Dean, College of Engineering and Computer Science

Robert W. Stackman Jr.
Robert W. Stackman Jr. (Nov 22, 2023 11:19 EST)
Robert W. Stackman Jr., Ph.D.
Dean, Graduate College

November 22, 2023
Date

ACKNOWLEDGMENTS

Sincere thanks go out to my committee members Dr. Imad Mahgoub and Dr. Ilyas for all their support and advice, and a particular shout-out goes to my advisor Dr. Waseem Asghar for his perseverance, tolerance, and encouragement during the complete process of research and write up of the thesis.

Finally, I want to express my sincere gratitude to my parents for all those years they spent helping me to pursue my education, my friends who always motivated me, and my lab mates for their moral support throughout the writing of my dissertation.

The author acknowledges support from TeleTech University in providing us with printed. motor by using their metal printer and support from the Department of Mechanical Engineering, Florida Atlantic University, Boca Raton, FL, USA for manufacturing Ti valve seat.

ABSTRACT

Author: Muhammad Waleed Anjum

Title: Development of An Automated Device for The Optimized Regulation of Cerebrospinal Fluid (CSF).

Institution: Florida Atlantic University

Thesis Advisor: Dr. Waseem Asghar

Degree: Master of Science

Year: 2023

Cerebrospinal fluid (CSF) has a role, in keeping the brain and spinal cord safe and nourished within the nervous system (CNS). This clear and colorless fluid is produced in the ventricles of the brain. Surrounds these structures acting as a protective cushion. CSF plays a role in maintaining nervous system health and ensuring optimal functioning.

CSF accomplishes four objectives.

Protection: The brain and spinal cord are shielded from harm due to CSFs natural shock absorbing properties. This effectively safeguards these structures, from injuries caused by impacts or collisions.

Nutrition

It ensures a favorable environment for neural cells to perform at their peak by supplying essential nutrients and removing waste products from the brain and spinal cord.

Homeostasis: CSF aids in preserving the central nervous system's chemical environment, ensuring that ions, pH, and other vital components are in appropriate balance. The regular flow and control of CSF, however, may be disturbed in several medical situations. One of the most frequent problems is hydrocephalus, a disorder marked by an abnormal buildup of CSF in the ventricles of the brain. If the pressure from the extra fluid is not managed, it may result in serious neurological issues and even life-threatening consequences. Medical innovation has produced a variety of gadgets and shunt systems to solve these problems and guarantee the regular function of the nervous system. These gadgets are made to regulate the amount of CSF, either by removing extra fluid or by promoting correct circulation. The treatment and management of disorders like hydrocephalus have considerably improved because of both historical and modern advancements in shunt systems and related technology. These advancements frequently entail the placement of specialized valves or shunts that control the flow of CSF and direct it away from the brain and spinal cord to another area of the body where it may be safely absorbed or expelled. By reducing the pressure brought on by extra CSF this method lets patients live more normally. Normal Intracranial pressure (ICP) is maintained in healthy individuals by the equilibrium between the rate of production and reabsorption which is a physiological inclination. However, if this equilibrium is disturbed the over drainage or under drainage may result. Over drainage results, if the production rate is lesser than the reabsorption rate, and under drainage results, if the production rate of CSF is more than reabsorption. By using a shunt system which is a low-resistance alternative

path, the abnormal ICP can be addressed. In this research, an automated shunt system is developed that can address the over and under-drainage problems by using onboard medical monitoring. This shunt system has the capability of external ventricular drainage (EVD).

DEDICATION

I dedicate this work to my parents and my wife.

DEVELOPMENT OF AN AUTOMATED DEVICE FOR OPTIMIZED REGULATION OF CEREBROSPINAL FLUID (CSF)

LIST OF TABLES

LIST OF FIGURES

LIST OF EQUATIONS

$$\text{CPP} = \text{MAP - ICP} = \frac{\text{Systolic Pressure}}{3} + \frac{2 \times \text{Systolic Pressure}}{3} \quad \ldots\ldots eq(1)$$

$$\text{Critical Pressure} = \text{Shunt Operating Pressure} + (R_{Shunt} \times \text{Infusion Rtae}) + 5mmhg \quad \ldots\ldots eq(2)$$

$$\text{PP} = ICP + HP - (OP \text{ or } CP) + IAP \quad \ldots\ldots eq(3)$$

$$K = \frac{Gd^4}{8D^3 n} \quad \ldots\ldots eq(4)$$

$$A_t = 2 \times \left(\frac{D\theta}{2} \right) \times l = D \times \theta \times l \quad \ldots\ldots eq.(5)$$

$$B_{ag} = \left(\frac{\phi_t}{A_t} \right) \quad \ldots\ldots eq.(6)$$

$$\phi_t = B_{ag} \times (D \times \theta \times l) \quad \ldots\ldots eq.(7)$$

$$\phi_p = \frac{\phi_t}{P} = \frac{B_{ag} \times (D \times \theta \times l)}{N_m} \quad \ldots\ldots eq.(8)$$

$$A_s = \frac{m \times (N_s / m) \times (2N_{tc}) \times (I_{cpms})}{D \times \theta} = \frac{2 \times m \times N_{tph} \times (I_{coil})}{D \times \theta} \quad \ldots\ldots eq.(9)$$

$$N_{tph} = \frac{N_s N_{tc}}{m} \quad \ldots\ldots eq.(10)$$

$$I_{coil} = \frac{A_s \times (D \times \theta)}{2m \times N_{tph}} \quad \text{.....eq.(11)}$$

$$\lambda_{\max} = K_w N_{tph} \phi_p \quad \text{.....eq.(12)}$$

$$\mathrm{E_{ph}} = \frac{d\lambda}{dt} = \frac{d\lambda}{d\theta_e} \times \frac{d\theta_e}{dt} = \frac{\lambda_{\max}}{\pi/2} \times \omega_e \quad \text{.....eq.(13)}$$

$$\mathrm{E_{ph}} = \frac{1}{\pi} K_w N_{tph} B_{ag} \times (D \times \theta \times l) \times \omega_m \quad \text{.....eq.(14)}$$

$$P_{out} = [\frac{1}{2\pi} K_w B_{ag} A_s \times (D^2 \times \theta^2 \times l) \times \omega_m] \quad \text{.....eq.(15)}$$

$$D = \sqrt[3]{\frac{P_{out}}{\frac{\tau}{2\pi} K_w B_{ag} A_s \times (\theta^2) \times \omega_m}} \quad \text{.....eq.(16)}$$

$$N_{tph} = \frac{A_s (D \times \theta)}{2 \times m \times I_{coil}} \quad \text{.....eq.(17)}$$

$$L_{pm} = \text{Length of permant magnent} = \frac{\mu_r \times B_{av} (g \times k_r)}{k_l \times B_r - (\frac{B_{av}}{C\phi})} \quad \text{.....eq.(18)}$$

$$W_{pm} = \text{Width of permant magnent} = \frac{D}{2} \theta_{\mathrm{m}} \quad \text{.....eq.(19)}$$

$$\sigma_{F\tan} = A\mathrm{B}\cos(\vartheta) \quad \text{.....eq.(20)}$$

$$D_{cond} = \text{Diameter of conductor} = \sqrt{\frac{4 \times A_{cond}}{\pi}} \quad \text{.....eq.(21)}$$

CSF Production(I_P) = CSF Storing + CSF Reabsorption(I_R).....*eq*.(22)

$$I_R = \frac{P(t) - P_{SS}}{R_{CSF}} \text{.....} eq.(23)$$

$$I_S = C\frac{dp}{dt} \text{.....} eq.(24)$$

$$Q = \frac{\Delta P \times \pi (R_o{}^2 - R_i{}^2)}{8\mu L}\left[(R_o{}^2 - R_i{}^2) - \frac{(R_o{}^2 - R_i{}^2)}{\ln\left(\frac{R_o}{R_i}\right)} \right] \text{.....} eq.(25)$$

INTRODUCTION

Cerebrospinal fluid (CSF) is a liquid that surrounds the brain and spinal cord. Its primary role is to transport nutrients and provide protection to the brain tissue. Before it circulates it drains into reservoirs located at the base of the brain. Hydrocephalus is a condition that occurs when there is a buildup of fluid (CSF), in the ventricles or spaces around the brain. CSF, which is a filtered version of plasma can be found in the ventricles of the brain and also in the spaces surrounding the skull and spine [2]. It plays roles in nourishing the brain eliminating waste and safeguarding it. Typically, five sixths of an adults 150 ml CSF volume is distributed across areas with one sixth residing in the ventricles. The production of CSF primarily takes place in the choroid plexus although other sources also contribute to some extent. In adults CSF production ranges from 400 to 600 ml, per day depending on each individuals factors. On average young adults undergo renewal of their CSF four to five times within a 24 hour period[3]. The conventional CSF shunt system is used to treat patients, with hydrocephalus and other neurological disorders. It regulates the drainage of fluid (CSF) from the brain into parts of the body such as the abdomen. This system comprises a shunt valve system, a distal/outlet catheter that directs CSF into the abdomen or other appropriate areas based on factors like age and the specific type of hydrocephalus and a ventricular catheter that provides access, to the CSF. Unlike blood, which circulates within blood vessels CSF is a fluid to plasma that surrounds the brain, spinal cord and central nervous system (CNS). During instances of brain trauma, fluid (CSF) is well known for its role, as a

cushion and shock absorber. It plays a role in maintaining blood flow and managing intracranial pressure (ICP). The main producer and secretor of CSF is the choroid plexus. When there are abnormalities in the generation, flow or absorption of CSF it can lead to increased pressure (ICP). Potentially cause hydrocephalus, which refers to an excessive accumulation of CSF, within the central nervous system (CNS)[1]. This condition is often accompanied by dilatation. Different levels of severity and chronicity of hydrocephalus can develop at any age. Neurosurgeons commonly see it as a primary disease or because of a variety of pathologies, including tumors, head injuries, brain hemorrhages, or infections[4]. Hydrocephalus may result from brain tumors obstructing CSF routes. 1% - 5% of patients with metastatic brain tumors and up to 10% of individuals with original brain tumors will develop hydrocephalus[5][6][7]. The most common type, communicating hydrocephalus, can be brought on by several things, including bleeding into ventricles during surgery, enriched CSF protein, radiotherapy-induced fibrosis of arachnoid granulations, or leptomeningeal dissemination of tumor cells. The most frequent surgical method for CSF diversion is a ventriculoperitoneal shunt (VPS), despite the operation's well-documented propensity for complications [8][6]. During the VPS surgery, a valve system is inserted to control the flow of CSF between ventricles to a distant compartment anywhere in the body. There are many commercially existing valve types, but none are more effective than the others in treating certain forms of hydrocephalus. The word shunt means to provide an alternative path of less resistance. Shunt is a term used in medicine to describe any procedure that gives a body fluid under pressure a better chance of escaping than it would if discharge were taking place naturally [1]. For the treatment of a patient who needs a ventriculoperitoneal shunt (VPS) or ventriculoarterial shunt (VAS), a shunt path

provided by the valve is often implanted subcutaneously together with its proximal and distal catheters. Other techniques include lumbar-peritoneal and ventriculopleural implantation.

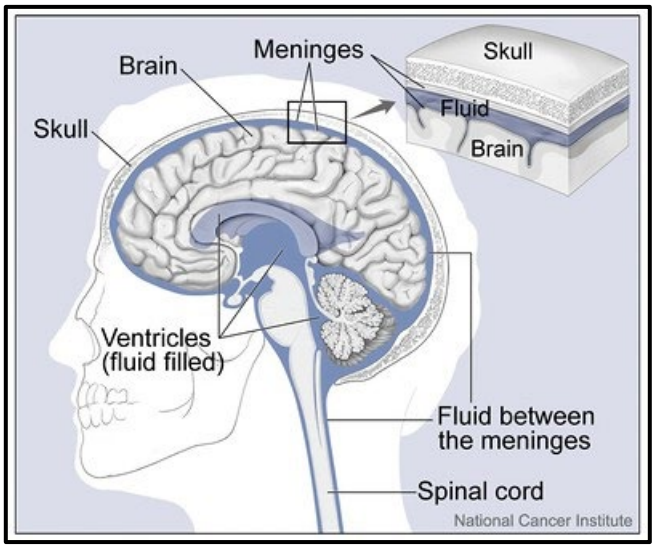

Figure-1. Brain Surrounded by CSF [9]

The brain's ventricles include a network of blood arteries called the choroid plexus epithelial cells, which are specialized ones. The synthesis of CSF is largely dependent on these epithelial cells. The choroid plexus epithelial cells actively move ions from the circulation into the ventricles, namely Na^+ (sodium), Cl^- (chloride), and HCO_3^- (bicarbonate), to produce CSF. Numerous ion transporters and channels found on the surface of these cells facilitates this process. Because epithelial cells are inherently polar, ions can only travel in one way. Because of this difference, in charge specific proteins responsible for transporting ions are found on both the surface facing the cavity (known as the membrane) and the surface facing the circulation (known as the basolateral membrane). In humans cerebrospinal fluid (CSF) plays a role in the fluid of the central nervous system. The CSF covers areas such, as the space, spinal canal and brain ventricles with a total volume of approximately 140. 150 ml (as shown in Figure

1). Cerebrospinal fluid (CSF) and neuronal tissue are separated anatomically by the pia mater, which covers the outside of the brain, and the ependyma, which lines the cerebral ventricles and canals[10]. The CSF fulfills several essential functions. Mechanical support is provided for the brain since the brain "floats" in the CSF, decreasing the weight almost to 60% (Segal, 1993). CSF also functions as the brain's drainage system by providing a "sink" where metabolic waste products or synaptic activity may be diluted before being excreted (Segal, 1993). Before reaching the CNS, certain nutrients may also pass via the CSF, according to Johanson (1999). According to Johanson (1999), the CSF may also act as a route for communication inside the CNS, carrying hormones and transmitters across distinct regions of the brain[10]. CSF mostly moves in one direction as it passes through the cisternal subarachnoid spaces that surround the brain and goes caudally via the ventricular system, giving the brain a sterile environment. It has been suggested that the CSF serves as a reservoir for cerebral extracellular fluid (ECF) because of the open communication between the extracellular fluid (ECF) of the neuropil and the CSF[11][12]. The choroid plexuses located inside the lateral ventricles secrete nearly 75% of the CSF in the human brain[13]. The ECF across the ependymal layer is responsible for 25% of the extra amount[14]. The juvenile human brain produces CSF at a rate of 340 ml/min, or approximately 500 ml/day [40, 45]. For the elderly, this drops to roughly 250 ml/day[15]. CSF is present in the adult brain in constant amounts of around 140 ml, of which 110 ml are found in the subarachnoid spaces and 30 ml are found in the ventricles[16]. As a result, every 24 hours, human CSF is replaced three times. The secretory mechanisms at the choroid plexuses and the arterio-venous pressure gradient both contribute to the steady flow of CSF inside the central nervous system[11]. Laminar flow and bulk flow must be

distinguished as two unique forms of flow since the processes are highly diverse and probably play quite different functions. Most of the cerebrospinal fluid (CSF) travels caudally, or downward, into the lower regions of the central nervous system, mostly to the fourth ventricle. The cerebral aqueduct, a unique channel that connects the third and fourth ventricles, is where this flow takes place. From there, it enters the subarachnoid space, which is composed of the brainstem and the cisternae magna and pots [17], either by the lateral Luschka apertures in all vertebrates of the sub-primate order or through the additional Magendie median aperture in primates alone[11]. The bulk of subarachnoid CSF flow seems to divide into cortical and lumbar components at the cisterna magna, with a minor amount of flow perhaps continuing via the spinal cord's central canal.[11] The cranial vault, which may be compared to a rigid, elastic cage, contains the brain, cerebral blood, and cerebrospinal fluid (CSF). Each of these parts of the brain produces an immediate pressure that modifies the volume of those structures. The intracranial pressure (ICP) that comes from these dynamics exhibits an exponential relationship with the fluctuations in volume (Vol) that each component goes through. This connection is extremely important. When considering the mechanics of CSF draining via a shunt device, this phenomenon becomes critical relevance. For patients undergoing neurosurgical and neurological operations, intracranial pressure (ICP) assessment is essential. Clinical signs linked to increased ICP, such as headaches, altered consciousness, and vomiting, are often regarded as inaccurate and not reliable markers of the illness. The threshold for increased ICP, which contributes significantly to subsequent brain injury and may indicate negative outcomes, is ICP > = 20 mm Hg. ICP monitoring may be helpful for several illnesses, including traumatic brain injury (TBI), intracerebral hemorrhage (ICEH), subarachnoid hemorrhage (SAH),

hydrocephalus, benign intracranial hypertension, meningitis, stroke, acute liver failure, and others [18][19]. For instance, the autoregulatory system may be compromised in some circumstances (such as head trauma or surgery and doing so could need using artificial ways to regulate ICP utilizing programmable shunt devices.

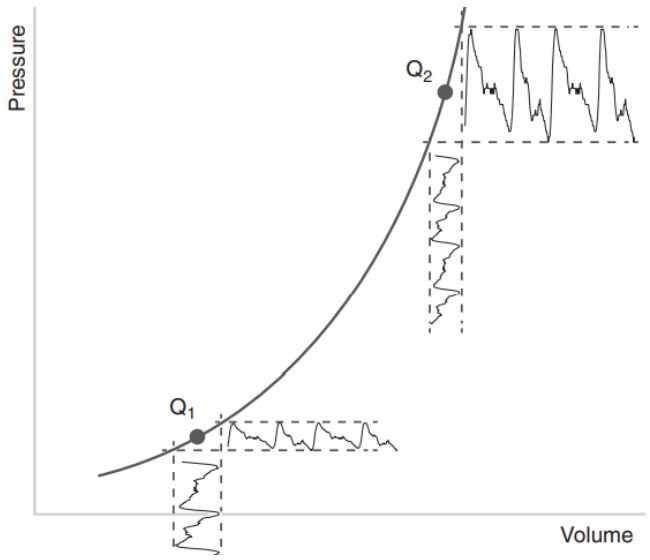

Figure-2 Nonlinear relation between increasing volume and pressure. At Varying Q a small increase in volume causes a marked increase in pressure.

$$\mathrm{CPP} = \mathrm{MAP} - \mathrm{ICP} = \frac{\text{Systolic Pressure}}{3} + \frac{2 \times \text{Systolic Pressure}}{3} \quad \text{.....} eq.(1)$$

Intracranial pressure (ICP) is commonly measured clinically to aid in the hydrocephalus diagnosis[20]. ICP and its constituent parts were examined to comprehend the dynamics of cerebrospinal fluid (CSF) better. The two techniques related to ICP measurement that are mentioned are a constant-rate infusion study and an overnight monitoring of ICP. The pressure and volume relationship may thus be better understood with longer-term ICP monitoring in combination with waveform assessment of ICP and cerebral autoregulation. The processing of intracranial pressure (ICP) data and an analysis based on a cerebrospinal fluid (CSF) circulation model are used in continuous-rate or overnight infusion research. This method is used to assess certain characteristics of cerebrospinal dynamics, such as passivity and CSF outflow resistance[20]. The brain is trapped in a rigid cage called a skull to protect it from external injury and shocks. An increase in intracranial pressure (ICP), which may reduce the blood flow, can lead to serious issues such as ischemia. The two sources of intracranial pressure are the abnormal circulation of cerebrospinal fluid and cerebral blood, or the "vascular component" and "circulatory component," respectively. Brain edema, vascular lesions, and CSF channel blockages all interfere with this circulation, which may cause the ICP to increase.

CONSTANT RATE INFUSION TEST

This method is based on measuring the intracranial pressure (ICP) response to a steady state level, by injecting a known amount of additional fluid (usually Hartmann's solution) into the cerebrospinal fluid (CSF) compartment. A lumbar puncture, a subcutaneously implanted reservoir linked to an intraventricular catheter, or a shunt pre-chamber may all be used to introduce fluid. A needle is required to connect the pressure transducer, while the other needle is required to connect the syringe infusion pump.

About ten minutes after the baseline pressure measurement, the infusion starts. The constant-rate infusion is stopped as soon as the ICP stabilizes (the plateau phase) or increases over the 40 mm Hg safety limit[21].

OVER-NIGHT ICP MONITORING

An established method for assessing the dynamics of cerebrospinal fluid (CSF) in patients exhibiting hydrocephalus-like symptoms is prolonged intracranial pressure (ICP) monitoring. Although a longer period (overnight) is desirable, supine monitoring is required for at least 30 minutes. It may be performed using a pre-implanted reservoir, an intraparenchymal probe which has different sections to measure local pressure, or by lumbar puncture. Lumbar puncture-measured pulse amplitudes were found to be somewhat less than intraparenchymal registration[22]. A pressure differential between the cerebral ventricles and the subarachnoid space is either nonexistent or very small in non-communicating hydrocephalus instances. However, research has shown that the ventricles' pulse pressure amplitude is higher than that of the subarachnoid space. An infusion study may be utilized to detect shunt deformities and gauge shunt effectiveness after shunting. Following a successful shunt, patients' preoperatively high levels of compensatory parameters should return to normal [23]. While the shunt is working correctly, the critical pressure given by the following formula shouldn't be exceeded[24].

$$\text{Critical Pressure} = \text{Shunt Operating Pressure} + (R_{Shunt} \times \text{Infusion Rtae}) + 5mmhg.....eq(2)$$

R_{Shunt} Denotes the hydrodynamic resistance of the opening shunt and a safety margin of 5 mmHg denotes a non-zero abdominal pressure.

According to the literature, CSF is secreted at a rate of around 0.35 ml/min on average. However, the real rate may differ significantly based on factors such as age and

hydrocephalus nature of communicating or non-communicating (0.007–0.45 mL/min) in children suffering from hydrocephalus having age between (5–13 Y), circadian rhythm, and other factors (such as REM sleep)[25][26]. When awake, the glymphatic system is considerably suppressed; when sleeping, it is stimulated. The parenchymal route of CSF absorption, in addition to the choroid plexus, plays a vital role in the secretions of CSF [27]. The hydrokinetic characteristics generally employed as benchmarks in the theoretical design of ventriculoperitoneal shunts may not be completely accurate when used in a device designed to drain cerebrospinal fluid (CSF) along an artificial channel that closely matches the cerebrospinal axis.[28]. The hydrostatic pressure gradient inside the catheter is determined by the vertical separation between the intake and output sites, not by the length of the catheter.

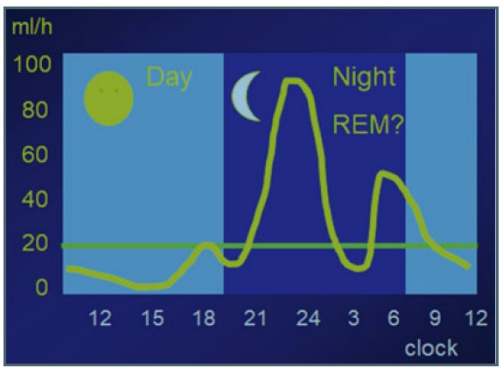

Figure 3: Formation of pressure gradient due to physiological variations in hydrostatic pressure

The main hydrokinetic force that significantly affects flow velocity and, consequently, the volume of fluid drained is the well-known "siphon" effect. The main force behind the motion is gravity. Internal pressure from the equilibrium of cerebrospinal fluid (CSF) production and absorption leads to an additional autonomous hydrokinetic force that impacts the flow, making it the second most important element after gravity[28].

The shunt device, intended to serve as a bypass mechanism during excessive CSF production, could not function if CSF production fell below absorption rates. As a result, any CSF that is retained inside the shunt tubes may lead to tube obstructions. Such an erratic operating pattern, characterized by intervals of inactivity and subsequent activation, is not thought to be effective for controlling intracranial pressure (ICP). This method is prone to clogs and presents contamination issues since the gadget could support bacterial growth. When the suction action causes the valve to open due to gravitational force, from the ventriculoperitoneal chamber, cerebrospinal fluid (CSF) flows downhill, depleting the ventricular chamber and perhaps leading to the collapse of the ventricles. As a result, cerebral hypotension may develop, which has been linked to the slit ventricle syndrome[29].

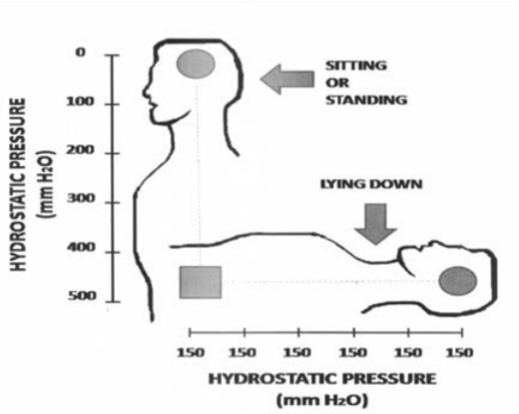

Figure-4: Variation of Pressure Due to Position[30]

The typical range for pressure (ICP) in adults is usually between 0 and 13.6 cmH2O with a threshold of 20.4 cmH2O considered within the range. If ICP consistently exceeds 28 cmH2O for a duration of 5 minutes, it indicates an increase in pressure which can be related to hydrocephalus. A condition characterized by an accumulation of fluid (CSF) in the brain's ventricles or subarachnoid space. Various factors such as

increased CSF production blockage in the ventricles and heightened ICP can contribute to the buildup of CSF potentially causing harm to brain structures. The severity of hydrocephalus determines the symptoms experienced by individuals affected including headaches, nausea, vomiting, vision issues, cognitive decline, mobility difficulties. In newborns specifically an enlarged head circumference is often observed[31]. Hydrocephalus can be classified into two types; hydrocephalus where CSF flows freely between ventricles and non-communicating hydrocephalus where there is obstruction in CSF flow. Another form known as pressure hydrocephalus (NPH) primarily affects individuals. Some possible causes for pressure include blockage in neck veins, airway obstruction, improper muscle relaxation, during medical procedures or surgeries hypoxia/hypercapnia (inadequate oxygen supply/accumulation of carbon dioxide) insufficient pain relief medication administration, incomplete sedation, state seizures, elevated body temperature and certain medications that cause cerebral vasodilation.

BACKGROUND AND MOTIVATION

The medical condition called "hydrocephalus" derives its name from the combination of the words "water" and "head." It is commonly referred to as "water, on the brain." The main characteristic of hydrocephalus is the accumulation of fluid in the brains ventricles or cavities. Hydrocephalus poses a life threatening risk. Affects over 1 million individuals in the United States. It's important to note that 1 in every 1000 newborns are born with hydrocephalus making it more prevalent than conditions such as spina bifida, brain tumors or Down syndrome. Unfortunately there is currently no cure, for hydrocephalus and no known method of prevention. The sole treatment option is brain surgery, and hydrocephalus is the main cause of pediatric brain surgery. The most common surgical treatment for hydrocephalus involves implanting a shunt, a kind of medical device. Shunt technology has not developed since the invention of the device, and it has one of the highest failure rates of any medical equipment now available on the market. In the first two years after installation, 50% of shunts are expected to fail, needing repeated neurosurgical operations. Over 10,000 kids are hospitalized in hospitals each year for shunt-related problems[32]. After birth, acquired hydrocephalus develops and is frequently caused by neurological conditions such as severe head traumas, intracranial tumors, cysts, intra-ventricular hemorrhages, or infections that damage the central nervous system (CNS).

TYPICAL SOURCES OF CONGENITAL HYDROCEPHALUS

Any kind of injury due to head collision has the potential to damage the brain's delicate structures, neurons, and vasculature. The cerebrospinal fluid (CSF) pathway may get contaminated with blood from damaged arteries, resulting in an inflammatory response. Furthermore, this may cause obstructions in the absorption of CSF because of the growth of scar tissue on the meninges or persistent blood cells. The area of the brain where brain tumors in children most often manifest is the posterior fossa. As a tumor grows it can expand into the Quartus, which disrupts the flow of cerebrospinal fluid (CSF) and leads to hydrocephalus. Hydrocephalus can also be caused by tumors in areas of the brain that obstruct or compress the system. Acquired. Is often preceded by ventricular hemorrhage, which is commonly observed in premature newborns. This condition occurs when the arachnoid villi, responsible, for absorbing CSF are blocked or when blood vessels along the lining rupture resulting in occlusion or fibrosis. The initiation of hydrocephalus is the outcome of the reduced CSF absorption. Meningitis is exemplified by the tenderness of the meninges, which are the shielding membranous coverings enveloping the brain and spinal cord. This condition is frequently triggered by a bacterial infection or less commonly viral infection. The disease may cause these crucial meningeal structures to become scarred, which might subsequently disrupt the cerebrospinal fluid (CSF) pathway[33].

The primary objective of this study is the creation of a unique shunt device with the idea of addressing the drawbacks of the existing CSF shunt devices. This research makes no claims about the therapeutic benefits of employing such a device above and beyond what a surgeon would suggest as the patient's primary course of therapy. This enhanced shunt aims to enhance its essential capabilities and give additional features by using cutting-edge design concepts. In the section above, the factors influencing CSF

production, intracranial pressure (ICP) regulation, and their dynamic behaviors are briefly covered.

The three types of anti-siphoning devices (ASD) are diaphragm-based, gravity-based, and flow-reduction devices. Anti-siphoning devices that reduce flow ASDs preserve an open state and provide sporadic flow control. However, these devices were unable to supply adequate flow when intracranial pressure rose at night. On the other hand, gravity and diaphragm devices exhibit patient positioning sensitivity. Diaphragm-based devices are very responsive to variation in external pressure and the orientation of the device concerning the bony protrusion situated on the temporal bone of the skull, situated on the sides of the head behind the ear, while gravitational devices are affected by the angle between the device's axis and the patient's head. The VP shunt forms a connection between the cerebral and intra-abdominal compartments when the apparatus is mounted vertically, acting as a siphon. There are one or two pressure-sensitive membranes that function as a diaphragm device at the distal catheter's upstream end. If the intracranial pressure (ICP), due to volume of cerebrospinal fluid at the inlet is greater than the ambient pressure, the diaphragm will not be attached to the crown seat. This design allows for the uninterrupted flow of cerebrospinal fluid (CSF) with in operating range of the device. The diaphragm will be pushed to the crown seat, sealing, and impeding the fluid channel, as indicated in Figure 5, when the pressure of CSF through the column of flow drops below atmospheric pressure due to the inverse relationship of pressure and volume. The perfusion pressure (PP) due to swelling or differential pressure across the valve due to physical change in the orientation, which may be computed using the following equation, controls the flow of CSF via the shunt.

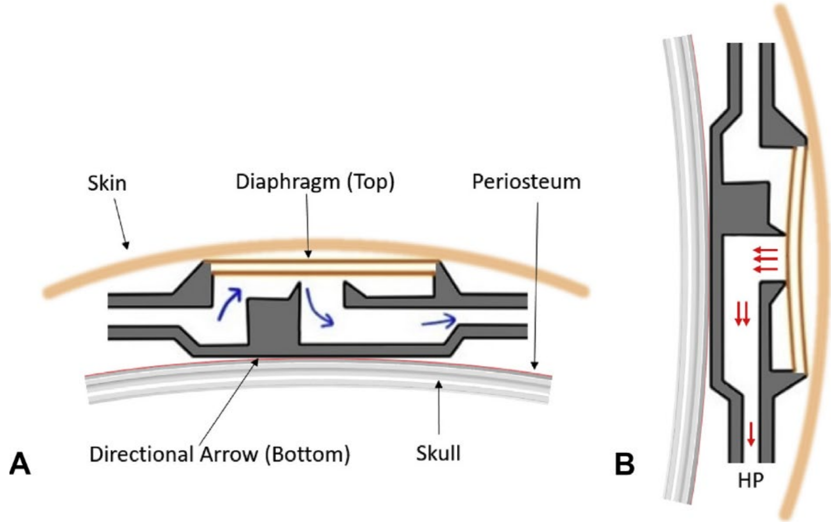

Figure 5: Diaphragm Valves [34]

$$\text{PP} = ICP + HP - (OP \text{ or } CP) + IAP \ldots\ldots eq(3)$$

Where, $HP = \rho gh$ denotes the hydrostatic pressure, $g = \text{gravitational constant} = 9.8\ \text{ms}^{-2}$ and $\rho = \text{fluid density}$, and "h" is the vertical height of the column, OP denotes the valve's opening pressure, CP denotes the valve's closing pressure, and IAP denotes intra-abdominal pressure. PP is determined by the OP in generally closed valves whereas it is expressed by CP in valves that are typically open. The volume of the CSF flowing per second which corresponds to a fluid rate of the CSF through the shunt system is calculated by the following equation. $Q = \frac{\Delta P}{R}$

$\Delta P = \text{Differential Pressure, and R} = \text{Resistance of system}$

The shift in all forms of pressure, including hydrostatic pressure (HP), intraabdominal pressure (IAP), and intracranial pressure (ICP), is what causes the variation in perfusion pressure (PP) owing to postural change in the ventriculoperitoneal shunt system. Figure 6 shows the difference between these values for a person resting supine and one who is sitting up straight (vertical).

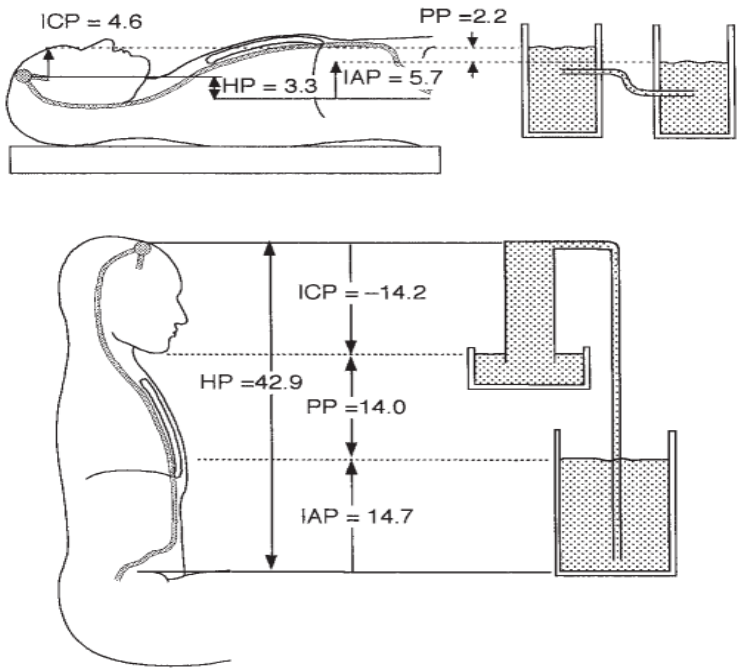

Figure 6: Variation of ICP, HP, IAP, and PP In Sitting and supine [35]

GRAVITATIONAL DEVICES

In this design, one or more metallic spheres are housed inside a titanium cylinder with a conical seating arrangement. When the device is upright, the metallic spheres are firmly resting on the conical surface, providing differential opening pressure (DOP), which is based on the weight of the spheres balancing the input of CSF.

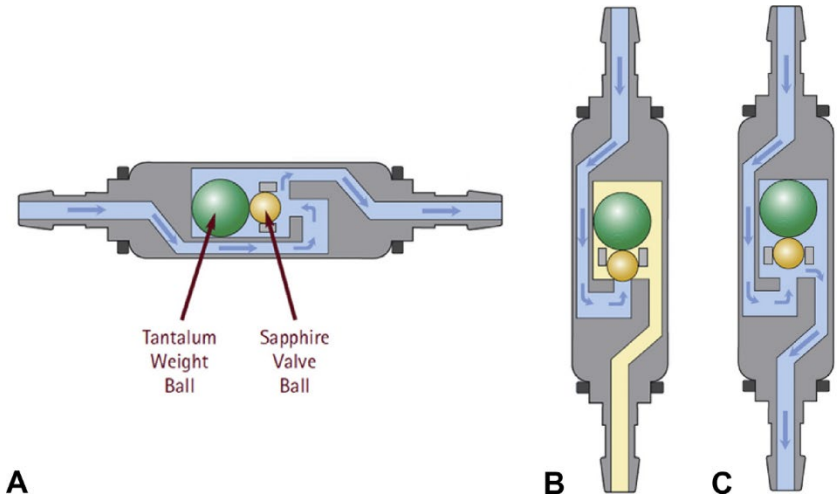

Figure 7: Gravitational Units [35]

FLOW REDUCING DEVICES

Devices that reduce flow are also referred to as "flow regulators". This specific device type aims to control flow based on differential Pressure (DP) which is the pressure between the inlet and outlet rather than variation in the postural change. As a result, it is not strictly speaking an "anti-siphon" gadget but, its purpose is to prevent the negative effects of over-drainage [25]. This group's lack of body position awareness is its most distinguishing characteristic. Its purpose is not fundamentally "anti-siphon," but rather flow reduction rather than a siphon effect counterbalance. Among the several shunt types available, programmable shunts stand out as superior to fixed pressure setting valves in that they allow for flexible adjustment of the opening pressure. To address concerns with over- or under-drainage, these programmable systems employ external magnets to change the position of the spiral cam, which regulates where the ball is put within the cone. Statistical data indicates that these programmable valves may need regular modifications

in response to patient comfort and symptom reports. The benefits and drawbacks of each kind of shunt valve are unique.

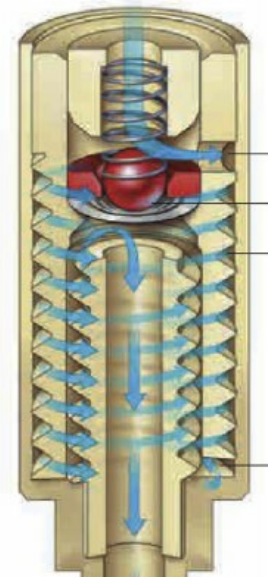

Figure 8: Effect of Gravity and Change in Path of Flow[35]

Although there are several great shunt devices on the market, there are certain inherent limits that must be understood. These include the potential for shunt obstruction brought on by impurities and the possibility of the positional change of magnets embossed on the rotor by ambient magnetic field interferences. Although unavoidable, these external magnetic field interferences may cause variations in the rate at which cerebrospinal fluid (CSF) drains. As a result, changes in drainage rates may be undetected by patients for a while. Patients often become aware of these modifications because of symptoms like headaches and intracranial pressure. It is impossible to exaggerate how vital it is to address these issues given that delaying would only increase the risk of potentially fatal consequences. In response to symptoms, medical professionals may suggest adjusting the valve settings, but there is no guarantee that the patient's condition will improve right

away with the new configuration. Additional conversations with the healthcare professional are often required to choose the best setting. Unwanted changes in valve settings may sometimes result from unexpected factors like mechanical shocks or the influence of ambient magnetic fields. These disturbances may lead to structural deformation of the valve and reduced cerebrospinal fluid (CSF) flow. Parts with rotating mechanics are prone to mechanical jamming by nature. Since it is difficult to replace these pieces after the shunt valve has been physically implanted, shunt valves containing such spinning components must undergo frequent upgrades. The potential for progressively accumulating debris, such as blood and protein-enriched fluids, can create blockage of the tiny catheter tube. The core issue with shunt clogs is this one. Due to the increased likelihood of early shunt blockage, a substantial number of surgeons have expressed concerns about implanting shunts in patients whose cerebrospinal fluid (CSF) contains an excessive amount of protein or red blood cells (RBCs).

RESEARCH OBJECTIVES

An electrically actuated ventriculoperitoneal (VP) shunt device is the main goal of this study, with a major emphasis on providing very effective hydrocephalus therapy. By enabling real-time intracranial pressure (ICP) monitoring and using sensory feedback mechanisms, this innovative technology is designed to improve patient care. With the use of this cutting-edge technology, it is hoped to proactively prevent brain damage brought on by hyper- or hypotension, therefore lessening the painful symptoms of hydrocephalus. As opposed to traditional shunt devices, which depend on consistent pressure settings for all patients, this new system's exceptional degree of customization and flexibility allows it to customize therapy to the unique needs of each patient. Real-time regulation of cerebrospinal fluid (CSF) flow rates is achieved with this cutting-edge technology, which also results in significant medical care cost savings. This system promises significant cost savings for both patients and healthcare providers by reducing the frequent need for traditional shunt reprogramming, revisions, and the risk of shunt blockage due to fluctuations in intra-ventricular pressure (IVP), intra-abdominal pressure (IAP), and hydrostatic pressure (HP), whether arising from over- or under-drainage. Additionally, it includes a user-friendly interface that makes it simpler to configure shunt settings, enabling long-term monitoring of a patient's CSF flow and intracranial pressure (ICP) behavior, largely for diagnostic reasons. Even in the presence of changing IVP, HP, and IAP circumstances brought on by changes in a patient's physical state and the dynamics

of the shunt system, the inclusion of an auto-adjustment mechanism guarantees the constant preservation of optimal shunt characteristics The system's attentive monitoring and warning features stand out as crucial protections against serious consequences resulting from inadequate or excessive CSF draining, playing a crucial part in improving patient safety and wellbeing. The unusual ball-in-cone design, which includes two essential components supported by a stainless-steel spring, is the foundation of the engineering of this electrically driven shunt device. The first reacts to increased cerebrospinal fluid (CSF) pressure levels and serves as an input for the shunt/bypass flow channel. Based on intracranial pressure dynamics, the valve opens when the CSF pressure exceeds a preset threshold. Greater CSF pressure on the ball compresses the spring, displacing it from the cone seat, and regulating the flow rate in either a downward or upward direction. The second element, which is arranged in an upside-down position, serves as a control valve. In this control valve, the ball's location concerning the cone seat may be changed by adjusting the harmonic motion of a plunger, which is driven by a specially created mini-stepping actuator. The CSF flow rate precisely controls the tiny stepping actuator's rotating motion in either a clockwise or counterclockwise direction, producing a dynamic reaction to changes in flow. This durable and finely constructed solution not only improves patient well-being from the standpoint of illness management but also maximizes time use. As a result of the removal of the time-consuming adjustment procedures involved with passive programmable shunt devices, patients may benefit from spending less time away from home. This design's real-time monitoring capability offers patients instant benefits in addition to providing medical experts with priceless information. Healthcare professionals may use the data patterns as crucial

information for prompt problem management and decision-making, providing a holistic solution that goes beyond simple symptom treatment.

MATERIAL SELECTION AND METHODS DEPLOYMENT

DESIGN CONSIDERATRION

The implanted device helps regulate the fluid (CSF) by diverting it away, from the fluid compartments near the spinal cord called ventricles. These fluid filled gaps, which are parts of the nervous system (CNS) make it easier for CSF to be transported to internal organs like the heart or stomach cavity. When dealing with conditions such as hydrocephalus, where there is a buildup of CSF in the brains ventricles due to blockages and increased pressure, inside the skull shunt devices are often used in treatment. These devices effectively transfer CSF from the brain to another part of the body the abdominal cavity, where it can be reabsorbed into the circulatory system through shunts. This treatment lowers intracranial pressure while safeguarding against neurological issues. The range of cerebrospinal fluid (CSF) flow and pressure settings for CSF shunts may vary depending on the kind of shunt and the patient's particular demands. These parameters are altered either during the surgical procedure or in subsequent postoperative visits to guarantee that the shunt appropriately maintains CSF pressure while guarding against over- or under-drainage. The average range for CSF flow via the shunt generally falls between 5 and 15 milliliters per hour (mL/Hr.) or greater, with rated pressures ranging from 10 cmH_2o to 30 cmH_2o. The patient's age, the kind of hydrocephalus, and the surgeon's clinical evaluation all have an impact on the appropriate flow rate selection.

The limitations associated with passive programmable shunts are as follows. Limited Adjustment: Passive programmable shunts may only be manually altered during in-person consultations. This may make patients feel uncomfortable, particularly if they need frequent adjustments due to changing CSF dynamics.

LACK OF REAL-TIME MONITORING

With these shunts, it is impossible to monitor the intracranial pressure (ICP) and CSF flow in real-time. As a result, changes in CSF outflow rates or pressure may not be noticed until the appearance of clinical symptoms, thereby delaying treatment.

DELAYED DIAGNOSIS

Issues like under-drainage or over-drainage, make it difficult to diagnose them and may necessitate waiting until the patient manifests symptoms or has post-operative follow-up, which may reduce the effectiveness of treatment.

Benefits of Advanced Shunt Systems with Sensory Capabilities: Sensory-enhanced shunt devices may wirelessly transmit data to healthcare professionals, allowing them to continuously monitor ICP and CSF flow and remotely monitor a patient's state. With no need for human adjustment, contemporary shunts may automatically modify their settings based on real-time data to optimize CSF drainage and pressure management. Passive shunt systems, which often depend on preset anti-siphoning mechanisms to manage intracranial pressure fluctuations, may have issues because of patient positioning and changes in intra-abdominal pressure. In certain situations, these shunts may struggle to make exact adjustments, which might lead to unexpected cerebrospinal fluid outflow rates. Contrarily, sensor-driven shunt systems provide a variety of advantages. These tools enable the evaluation of the monitoring of intracranial pressure

(ICP) and cerebrospinal fluid (CSF) in real-time and control the flow rate, allowing dynamic adjustments in response to real-time data.

DESIGN AND OPERATION

A sophisticated shunt device with sensory feedback and flow control capabilities has been created to help with the automated regulation of cerebrospinal fluid (CSF) depending on the current conditions, including pressure and flow values. A Sensirion LPG 10-1000 flow sensor, with a full-scale flow rate $1000 \mu L$ and an output limit, $1500 \mu L$ is integrated into the prototyped design. Additionally, an actuator is used to provide translational motion, to a plunger coupled to a ball inside a conical structure, using a specially designed mini-stepping actuator, with six separate operating stages, as shown in the figure 9. The spherical ball has a stainless-steel spring attached to it. The flow rate of the fluid is subsequently affected by the plunger's movement into the control cone, which modifies the CSF's accessible space in the cone. Changes in CSF production levels, changes in body position (such as lying down, sitting, and standing), differences in how well other physiological tissues absorb shocks, and mechanical shocks are only a few of the variables that affect the flow rate. Due to its corrosion resistance properties, titanium was used to make both the cones, control cone, and inflow cone while stainless steel was used for the spring that is part of the assembly. The input signal for the motor's rotational control is the detected flow rate, guaranteeing exact synchronization with the plunger's translational motion. By controlling the distance between the ball's base and the cone's inner perimeter annular region, this coordinated motion regulates the flow rate and achieves the necessary flow control. The structure of the cone has been methodically

created and produced because of several tests in the field of flow management using conical structures with tapered inner surfaces behaving as annular regions. A spherical ball's curvature is perfectly aligned with the inside configuration of this special cone, which was carefully manufactured. An expertly built seating configuration is produced because of the deliberate conformance between the ball's curve and the cone's inner shape. Due to this accuracy, the fluid flow is effectively stopped anytime the ball and cone's curvatures are perfectly aligned. This creative design provides a highly accurate and dependable way to manage fluid flow in the fabrication of shunt devices. The pressure conditions at the proximal side, which serves as the shunt's designated inlet or inflow cone, determine how the shunt device will function. The ball within the cone in this mechanism moves out of its position when the pressure rises over the preset opening pressure (OP). The efflux of fluid is then methodically controlled by a control cone, which precisely controls the flow rate by using the auto-flow regulation mechanism of the proposed shunt device.

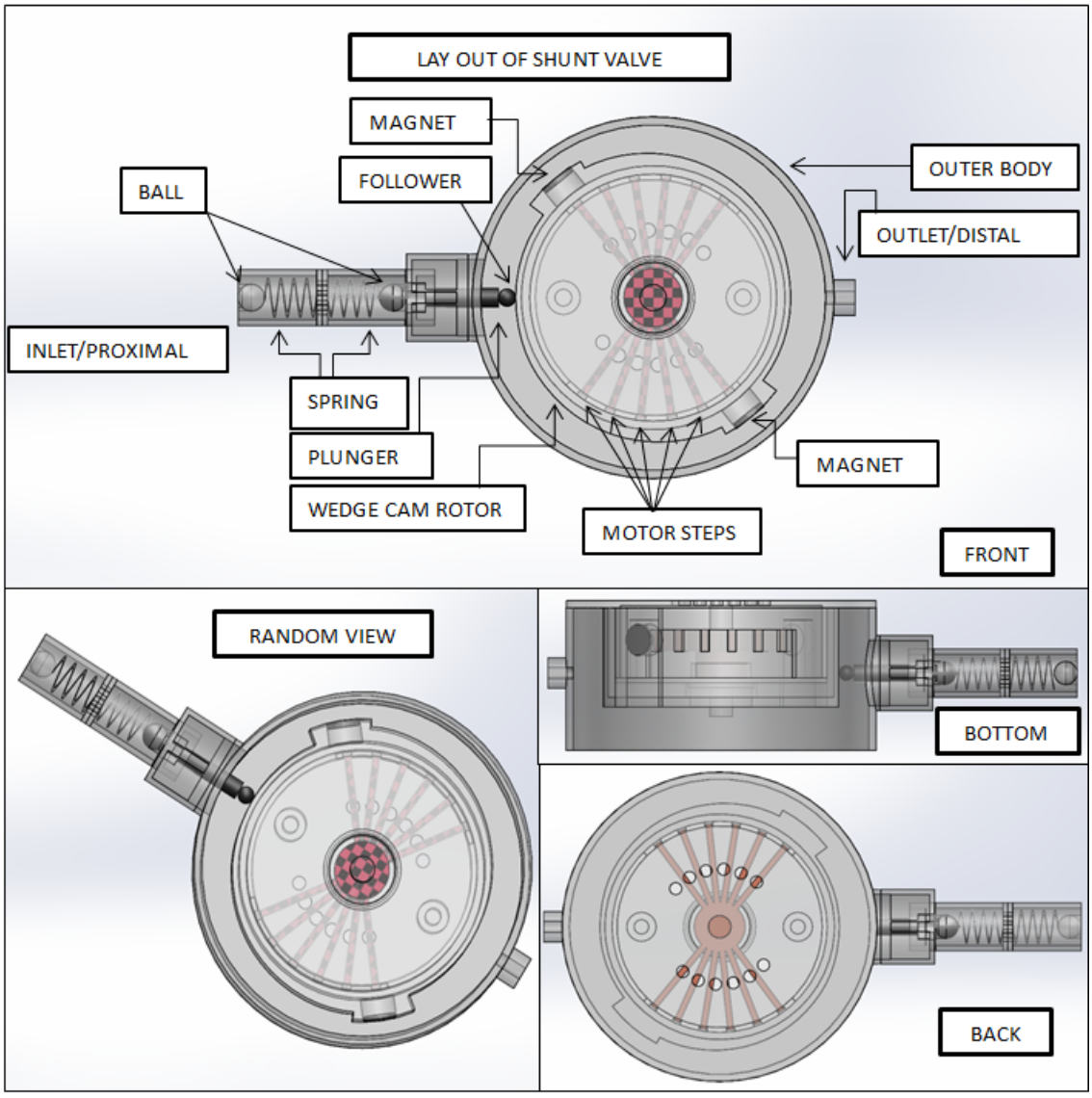

Figure-9: Geometrical View of Designed Shunt Device

In this arrangement, a critical structural element is a spring made of stainless steel (SS), which is anchored at one end by a solid support and at the other by a precisely placed ball that is nestled inside of a cone. The motor's output power and the desired flow rate are both considered when calculating the spring constant, guaranteeing smooth system functioning. A fail-safe method has been seamlessly included to protect against probable problems with the active adjustment system, such as motor failure or the appearance of

hydrodynamic impediments. This backup plan enables the use of an external magnet to start the motor's spinning component. The system also has a built-in notification mechanism that alerts users as soon as such accidents occur, ensuring uninterrupted operation by smoothly switching into a passive shunt mode. It is very helpful because this device can sustain the continuous circulation of cerebrospinal fluid (CSF) for an extended operating duration. This circulation is made possible by the dynamic mechanism by which CSF enters the ball-in-cone valve and subsequently exits the valve chamber to accommodate volume changes. Notably, the high-pressure fluid flow also serves as a directed pump, reducing the likelihood of blockages and obstructions in the internal components of the shunt, including the proximal and distal catheters. The device's many functions considerably increase its robustness and reliability in clinical applications.

CONCEPTION AND ACTUALIZATION OF PROTOTYPE

This investigation was based on the first experimental setup, which was built to evaluate the performance of the micro-stepping actuator that was used to actuate the ball-in-cone valve. To close the gap between the theoretical idea and its actual implementation, the framework must be thoroughly dissected, and complex factors must be evaluated to meet the predefined goal. Figure 10 illustrates the primarily developed prototype, a crucial stage in the execution of our central idea: the creation of a personalized tiny stepping actuator. In this first design iteration, we wrapped coils around two iron nails that had been carefully fastened within a 3D-printed model to ensure structural integrity. 600 turns of 38 AWG wire were painstakingly coiled around these two iron nails, which were spaced apart by about 30 degrees, to produce an effective electromagnet. These

coils were deliberately arranged in a 90-degree circle into four segments. These vital parts were encased inside the 3D-printed structure to protect them and provide insulation against any water exposure.

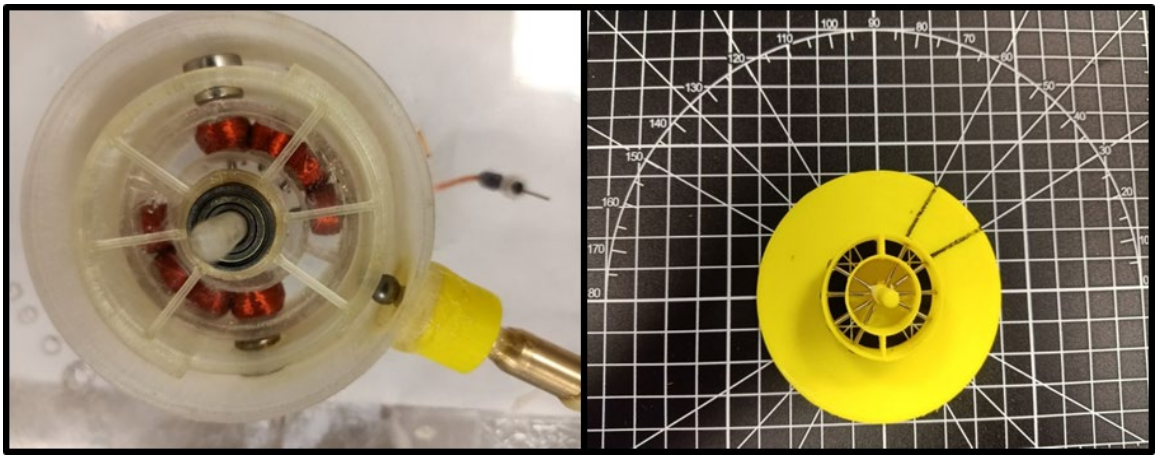

Figure-10: Geometrical View of 1st Designed Mini Stepping Actuator

Because the qualities of nano-pure water closely resemble those of cerebrospinal fluid (CSF), we chose to utilize it in our experiment to ensure the accuracy of our findings. Precision bearings enable the pivotal rotating component of the motor to operate around the central shaft. A pair of magnets that are carefully positioned 180 degrees apart are integrated into this rotatable piece that was painstakingly created via 3D printing. This design's idea was to make use of electromagnetic force, which would cause magnets to be dragged inexorably toward powered electromagnets. This motor part's varying thickness gives it a distinguishing snail-shaped cam look. It is positioned at an angle of 180 degrees and is flawlessly merged with the rotor to create a single, cohesive unit. When the magnet aligns with the first coil, this thickness displays a continuum, beginning at zero and gradually rising to its maximum thickness as the magnet moves forward to line with the fourth coil. This exact measurement is calibrated to work in

harmony with the cone seat's shape, guaranteeing smooth and precise motor functioning. We used the ferromagnetic qualities of iron nails when they were near a magnet to keep the rotor steady in the absence of an electromagnetic field produced by electromagnets because of current flow.

Figure-11: Geometrical View of Cone with and Without Ball

The rotor ’s-controlled immobilization was made possible by this configuration. Figure 9 displays a well-crafted aluminum plunger that is intelligently encased inside a 3D-printed structure that expertly fills the job of a follower or guide. Aluminum selection for the plunger material has a strong reason behind it, which is aluminum is a non-magnet. If any material has magnetic properties it may interfere with a magnetic field of permanent magnet used on the rotor as well as with the magnetic field of the electromagnet. The plunger has a symmetrical attachment at one extremity to the titanium cone's base and a connection to a stainless-steel ball at the other. To reduce resistance when the stainless-steel ball interacts with the finely crafted snail-shaped cam, the stainless-steel ball was strategically added beside the plunger. A regulated movement occurs within the cone because of the follower and plunger's harmonic

interplay. The snail-shaped cam gradually changes, thickens, and spins in an organized fashion, applying perfectly controlled pressure to the attached ball via a well-coordinated sequence of movements. This coordinated motion therefore exerts a compelling force on the ball within the cone, guaranteeing rigorous control over fluid flow in strict accordance with the set specifications. Cerebrospinal fluid (CSF) may flow because of the clearing channel made when the ball is raised from its position within the cone. A higher flow rate results from this expanded fluid passageway. Notably, the spring mechanism on the ball within the cone was purposefully chosen to act as a restoring force. Since the restoring force is inversely proportional to the spring constant, fluid flow dynamics are met with a dynamic and flexible reaction. On the other hand, the spring's restoring force is activated when the snail-shaped cam spins in the direction of decreasing thickness, pushing the ball within the cone toward the cone seat. The flow rate gradually decreased because of this movement, which successfully reduced the gap area between the ball and the seat of the cone as shown in Figure 12.

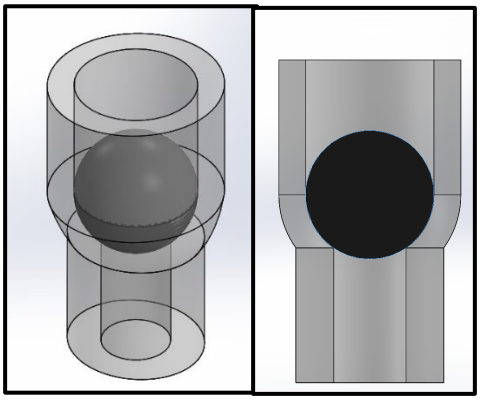

Figure-12: Geometrical and Cross-sectional View of Ball In Cone To Illustrate The Concept of Clearance Area

The Sensirion LPG-10-1000 flow sensor, a vital part of the system's real-time control, is included to permit the precise monitoring of the flow rate. It is interesting that the

motor, which was made of iron nails, requires a 20 Volt power source to effectively provide the necessary full-load torque. The degree of the full load torque has a complex relationship with the spring constant, highlighting the interconnectedness of two vital system variables.

SPRING SELECTION

The spring constant (K) and the rotor moment of inertia play important roles in determining the output power of the motor. As a result, a key factor in the motor's effective operation was the choice of an ideal spring. Several important aspects play a critical role in determining the spring's appropriateness, which necessitates a low amount of force for both compression and extension. These include a larger number of coils within the spring, the use of thinner wire, and the reduction of travel distance. The outer diameter (OD) of the spring rises in direct proportion to its appropriateness. The following mathematical connection, which is influenced by the parameters, governs the calculation of the spring constant: $K = \frac{Gd^4}{8D^3n}$ .....*eq*(4)

Where, G = Shear modulus of the material used (SS)

d = Wire Guage Diameter

D = Coil Diameter

n = Coil Rings Numbers

Different springs that were tested ranged from (k = 30 to 55 N/m). The final spring utilized in 2nd cone had a spring constant of 52.89 N/m, and this value gives a starting point for the designing of the mini-stepping actuator.

MOTOR DESIGNING

The choice was made to forgo using pre-manufactured miniature motors or other actuators, which frequently include integrated controllers, to adhere to strict criteria encompassing dimensional considerations, current rating, power rating, and voltage rating, with a primary focus on maximizing battery life or minimizing power consumption. This purposeful decision prevents the shunt device from growing excessively large. A custom mini-stepping actuator was painstakingly built to achieve the performance characteristics listed above. The integration of six electromagnetic coils, as seen in the accompanying image, is a distinguishing characteristic of this stepping actuator. The motor can do discrete step rotations of 15 degrees each because these coils are arranged at angular intervals of 15 degrees. Two compact disc magnets, enclosed in an assembly that is firmly fastened to a shaft and bearings, enable this rotating movement. These magnets act as the engine for the body's rotation when the coils are activated. The following equations were used in the design of the mini-stepping actuator.

DERIVATION OF EQUATION FOR MOTOR DESIGNING

P = No. of poles = N_m

N_s = No. of stator teeths

Area of teeth

$$A_t = 2 \times \left(\frac{D\theta}{2} \right) \times l = D \times \theta \times l \qquad \text{.....eq.(5)}$$

Air gap flux density:

$$B_{ag} = \left(\frac{\phi_t}{A_t} \right) \qquad \text{.....eq.(6)}$$

Rearranging the above equation for flux provided by the teeth:

$$\phi_t = B_{ag} \times A_t$$
$$\phi_t = B_{ag} \times (D \times \theta \times l) \qquad \text{.....eq.(7)}$$

Flux of the pole:

$$\phi_p = \frac{\phi_t}{P} = \frac{B_{ag} \times (D \times \theta \times l)}{N_m} \qquad \text{.....eq.(8)}$$

Electric Loading:

$$A_s = \frac{\text{Total Ameper Turns}}{\text{Perimeter}}$$
$$A_s = \frac{m \times (N_s / m) \times (2N_{tc}) \times (I_{cpms})}{D \times \theta} = \frac{2 \times m \times N_{tph} \times (I_{coil})}{D \times \theta} \qquad \text{.....eq.(9)}$$
$$N_{tph} = \frac{N_s N_{tc}}{m} \qquad \text{.....eq.(10)}$$

Rearranging equation. (5) for the current of the coil:

$$I_{coil} = \frac{A_s \times (D \times \theta)}{2m \times N_{tph}} \qquad \text{.....eq.(11)}$$

$$\lambda_{\max} = K_w N_{tph} \phi_p \qquad \text{.....eq.(12)}$$

Emf of the phase given by the rate of change of the flux:

$$\mathrm{E_{ph}} = \frac{d\lambda}{dt} = \frac{d\lambda}{d\theta_e} \times \frac{d\theta_e}{dt} = \frac{\lambda_{\max}}{\pi / 2} \times \omega_e \qquad \text{.....eq.(13)}$$

By putting the value of $\lambda_{\max}$ from equation (8) and solving for $\mathrm{E_{ph}}$

$$\mathrm{E_{ph}} = \frac{2}{\pi} K_w N_{tph} \phi_p \times \omega_m \times \frac{p}{2} \qquad \therefore P = N_m$$

$$\mathrm{E_{ph}} = \frac{N_m}{\pi} K_w N_{tph} \frac{B_{ag} \times (D \times \theta \times l)}{N_m} \times \omega_m$$

$$\mathrm{E_{ph}} = \frac{1}{\pi} K_w N_{tph} B_{ag} \times (D \times \theta \times l) \times \omega_m \quad \text{.....eq.(14)}$$

Based on the output power of the motor, which is required, the input power can be calculated as:

P_{out} = Required Value

$$P_{in} = \frac{P_{out}}{\eta}$$

$$I_t = \frac{P_{in}}{V_{dc}}; \qquad \text{Average Terminal Current}$$

$$I_{coil} = \frac{I_t}{N_p} \qquad \text{where } N_p = \text{ Number of parallel paths in winding,}$$

which is one in our case, so $I_{coil} = I_t$

For the calculation of P_{out}:

$$P_{out} = m \times \mathrm{E_{ph}} \times \mathrm{I_{coil}} = m[\frac{1}{\pi} K_w N_{tph} B_{ag} \times (D \times \theta \times l) \times \omega_m][\frac{A_s \times (D \times \theta)}{2m \times N_{tph}}]$$

$$P_{out} = [\frac{1}{2\pi} K_w B_{ag} A_s \times (D^2 \times \theta^2 \times l) \times \omega_m] \quad \text{.....eq.(15)}$$

Aspect Ratio of machine, $\tau = \frac{l}{D}$ Solving for $D^2 L$ from equation (15)

$$D^2 L = \frac{P_{out}}{\frac{1}{2\pi} K_w B_{ag} A_s \times (\theta^2) \times \omega_m} = D^2 (\tau \times D) = \frac{P_{out}}{\frac{1}{2\pi} K_w B_{ag} A_s \times (\theta^2) \times \omega_m}$$

$$D^3 \times \tau = \frac{P_{out}}{\frac{1}{2\pi} K_w B_{ag} A_s \times (\theta^2) \times \omega_m}$$

$$D = \sqrt[3]{\frac{P_{out}}{\frac{\tau}{2\pi} K_w B_{ag} A_s \times (\theta^2) \times \omega_m}} \quad \text{.....eq.(16)}$$

For N_{tc} calculation, rearrangement of N_{tph} from equation (5):

$$A_s = \frac{2 \times m \times N_{tph} \times (I_{coil})}{D \times \theta}$$

$$N_{tph} = \frac{A_s (D \times \theta)}{2 \times m \times I_{coil}} \quad \text{.....eq.(17)}$$

Permanent Magnet Dimensioning:

User-defined air gap:

$$L_{pm} = \text{Length of permant magnent} = \frac{\mu_r \times B_{av} (g \times k_r)}{k_l \times B_r - (\frac{B_{av}}{C\phi})} \quad \text{.....eq.(18)}$$

VALIDATION OF MOTOR DESIGN EQUATION:

The radius of a rotor which is attached to a hemispherical cam used for giving translational to a plunger is 23 mm, the stainless spring used has a spring constant of 52.89 N/m. The maximum displacement by which the spring is to be compressed by the rotor of mini stepping actuator is 2 mm. The value of the spring constant and maximum compression of spring helped in finding out the restoring force of spring calculated by F_r = -Kx .

The span covered by the six consecutive coils, which serve as six steps of the actuator, is 90º. The mechanical angle between these consecutive coils is 15º found by using the equation. The time taken to complete one step came out 0.50 milliseconds. To complete one revolution or 360º it took 12 milliseconds. According to these values, in one minute

stepping actuator will make 5000 revolutions. Figure-7 shows the current drawn by the mini stepping actuator is 0.5 A and the time taken to complete one step is 0.0005 s.

$$\theta_{\mathrm{m}} = \frac{\text{span}}{\text{steps}} = \frac{90}{6} = 15^{o} = 0.2618\, rad$$

The torque required to compress the spring having constant 52.89 N/m by 2 mm comes out to be 0.0023 N m. The outer stator diameter of the core calculated by equation (16) is 46 mm. These values can be seen in Table 1, These values are obtained from the solution of the motor-designed equation in MATLAB, and the figure-7 the result of the simulation performed in FEM.

$$D = \sqrt[3]{\frac{P_{out}}{\frac{\tau}{2\pi} K_w B_{ag} A_s \times (\theta^2) \times \omega_m}} \qquad \text{.....eq.(16)}$$

The length of teeth from the aspect ratio and outer stator diameter, calculated by the above-mentioned equation is $l = \tau \times D \ = 4\text{mm}$

The number of turns per phase calculated by using equation 17 comes out to be 458.

$$N_{tph} = \frac{A_s (D \times \theta)}{2 \times m \times I_{coil}} \qquad \text{.....eq.(17)}$$

The number of turns per coil calculated by using equation 10 comes out to be 229. The length of the permanent magnet calculated by using equation 18 comes out to be 3 mm.

$$L_{pm} = \text{Length of permant magnent} = \frac{\mu_r \times B_{av} (g \times k_r)}{k_l \times B_r - (\frac{B_{av}}{C\phi})} \qquad \text{.....eq.(18)}$$

The width of the permanent magnet is calculated by using equation 19 is 6 mm.

$$W_{pm} = \text{Width of permant magnent} = \frac{D}{2} \theta_{\mathrm{m}} \qquad \text{.....eq.(19)}$$

$$\sigma_{F\tan} = A\mathrm{B}\cos(\vartheta) \quad \text{.....eq.(20)}$$

$$\tau = \sigma_{F\tan} \times volume = \sigma_{F\tan} \times A_{surface} \times r = \sigma_{F\tan} \times 2(r\theta l) \times r$$

$$\tau = \sigma_{F\tan} \times 2(r^2 \times \theta \times l)$$

Current Density: The current per square meter area of wire is represented by J having a value of 15.5 A/mm^2.

$$A_{cond} = \text{Area of conductor} = \pi \frac{D_{cond}^{\ 2}}{4}$$

$$D_{cond} = \text{Diameter of conductor} = \sqrt{\frac{4 \times A_{cond}}{\pi}} \quad \text{.....eq.(21)}$$

Coil arrangement and current drawn by the coils are calculated from the design equations and verified by the finite element method software FEM and shown in Figure 13.

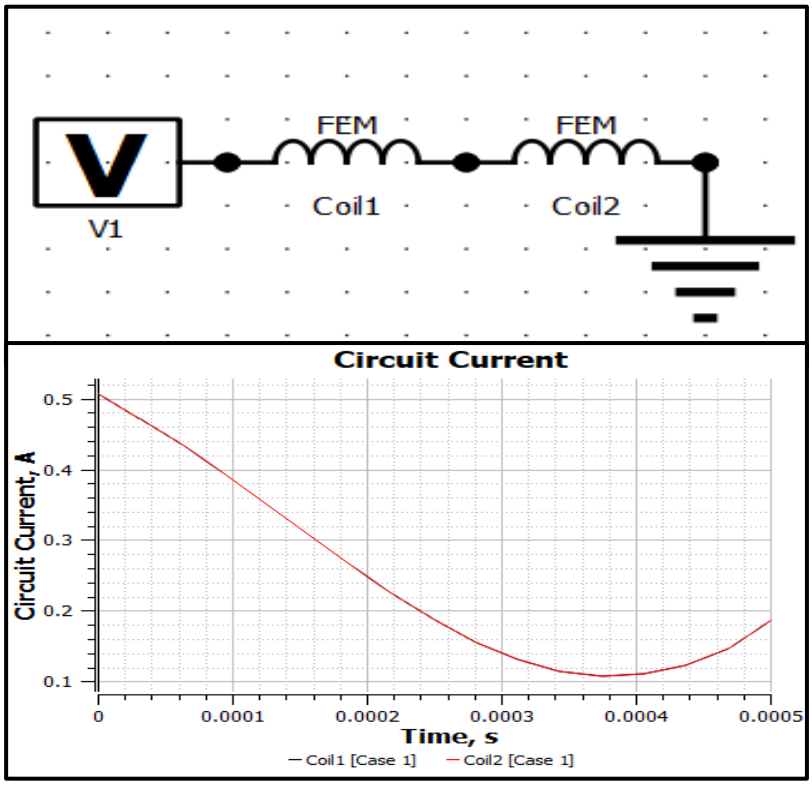

Figure-13: Coil Connection Arrangement and Graph of Current Flowing Through Them in One Cycle of Energization

The torque provided by the rotor of the mini-stepping actuator, while rotating through one step is proved from the results of the simulation performed in FEM. The value of the torque follows the one calculated by the mini-stepping actuator design equation result and its value can be seen from the graph in figure 14.

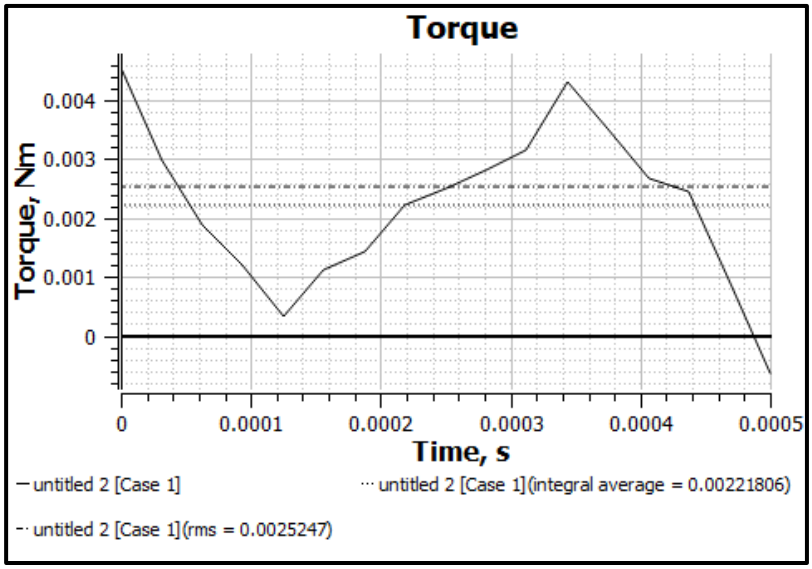

Figure-14: Average Torque Produced by Energization of One Coil

The proof of the rotational distance traversed by the rotor in one step is shown in Figure 15 and this graph is the result of the simulation performed in FEM.

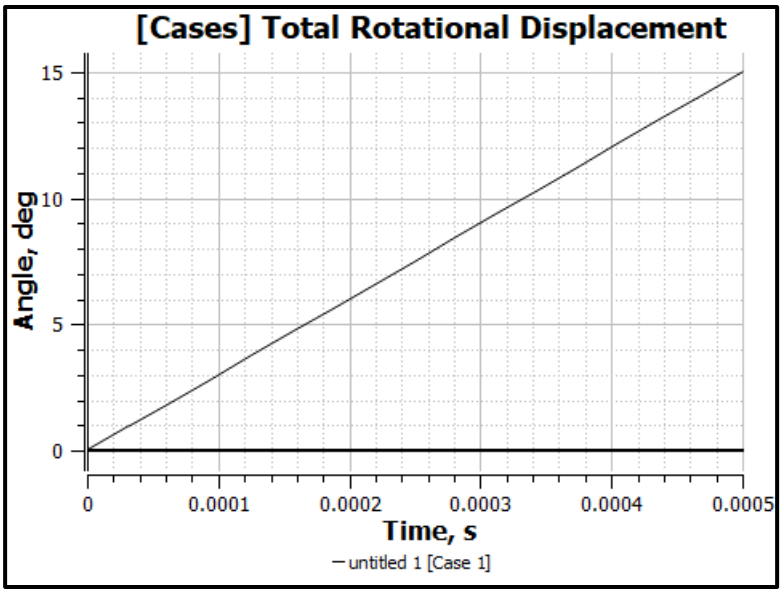

Figure 15: Angle Subtended by The Rotor In One Step

The results of the rotational velocity of a mini stepping actuator by the design equation and graph obtained by the simulation from FEM are the same and are shown in Figure 16.

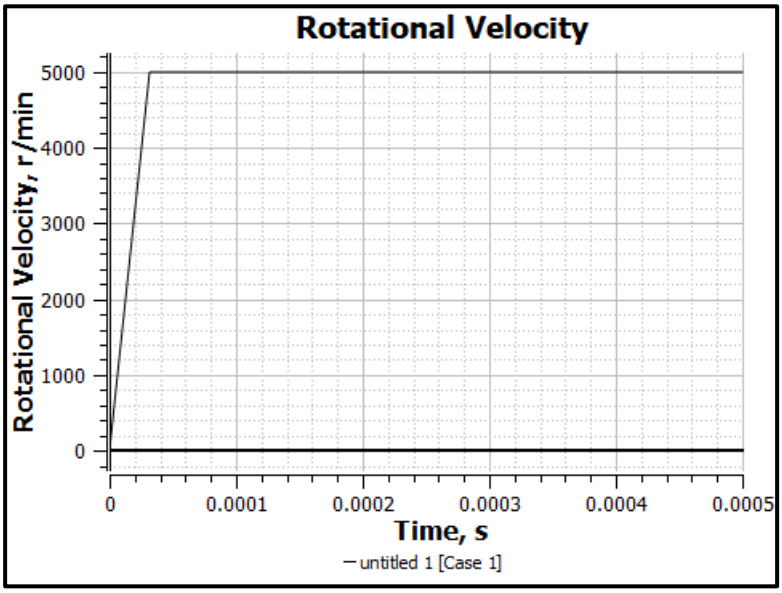

Figure 16: Rotational Velocity (ω) The Rotor in One Step

The results of all the variables that are used in the motor design equation are calculated by solving the equations in MATLAB and are presented in table 1. The letters used for

representing these variables have different terminologies which can be seen for more understanding in the code provided at the end. Every equation has comments on it to understand the meaning of the term.

VARIABLE	VALUE	VARIABLE	VALUE	VARIABLE	VALUE
B_{avg}	0.7000	D	0.046	I_{ph-pk}	0.500
Torque	0.0023	W_rpm	5000	I_t	0.500
B_r	1.4	g	0.0020	Tau	0.0014
C_phi	1	I_{c-pk}	0.500	N_p	1
K_r	1.1	l	0.0040	Mu_r	1.05
K_l	0.90	L_pm	0.0029	N_m	2
Kw	0.95	m	1	N_s	2
N_{tc}	228.81	Span	90	Theta_m	0.2618
N_{tph}	457.62	Steps	6	As	38000
P_{in}	0.0025	tau	0.0869	V_{dc}	5
P_{out}	0.0012	Theta	15	w	523.59
Efficiency	0.4800	W_rps	83.33	W_m	0.0060

Table 1: Values of All Parameters Used for Designing Mini Stepping Actuator

ANALYSIS OF DESIGNED MOTOR BY FINITE ELEMENT METHOD (FEM)

Using SolidWorks software, the exact shape of the small stepping actuator was carefully created, with numerical values for variables/parameters generated from the equations.

Using finite element method (FEM) software, a thorough simulation of the motor's design was painstakingly carried out, and the results conclusively proved its functional effectiveness. The motor's core was then created using a metal 3D printer, mirroring this cautiously detailed design, but with surface flaws caused by the required supports of structures during the printing process. Figure 17 displays the post-processing condition (After Filing).

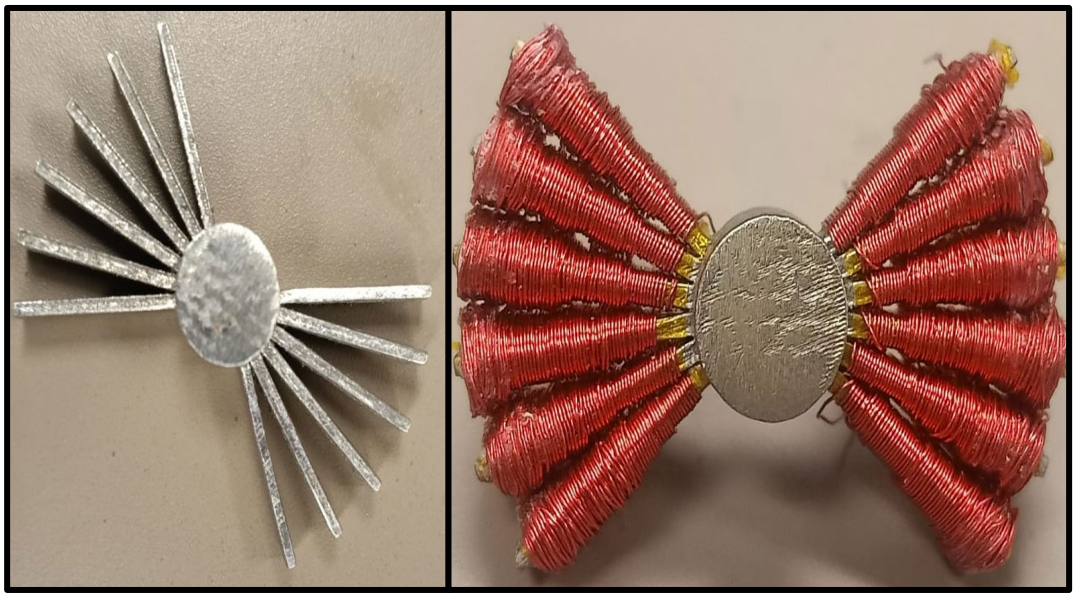

Figure 17: Unwind Core After Filing and Winded Core

The insulated wire was cautiously coiled by hand around the ferromagnetic core after core filing. The image shows the tightly coiled core for precise computation of the number of turns required due to the closeness of the core's legs. A printed circuit board (PCB) was wisely used to join the coils and provide smooth connections. A 3D-printed protective shell was placed around the PCB assembly and electromagnetic coils to guarantee electrical isolation from the surrounding fluid environment. The magnetic field interaction between the disk magnets and electromagnets took place at the

magnetically important end face of the core's legs. The whole system was epoxy-coated as an added layer of security and to improve electrical insulation.

The interaction between disk magnets and electromagnets can also be seen from the simulation results obtained from the finite element method (FEM). The values of magnetic field density with and without the coil energization vary and can be seen from the figure. In the 1st position core, teeth, and magnets are shown by a green color and the magnetic flux density of the magnet passes through the core. The 2nd position of the core teeth is shown with a coil on it in purple color and its flux density is zero because the coil is not energized. The rotor is held suspended by the magnetic locking of core teeth and magnet. The rotor will not rotate in this state even with the orientational change, or any mechanical jerk of the shunt device.

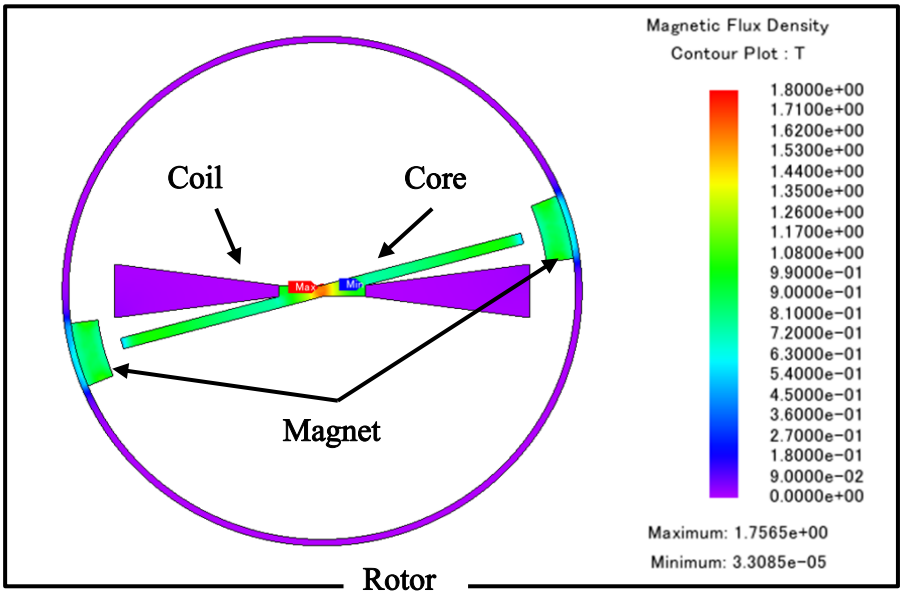

Figure 18: Simulation Result of Interaction Between Magnet and Coil

In Figure 19 on the next page, the purple-colored coil is removed from the core teeth intentionally to see the magnetic flux density of the magnet flux linkage with 2nd teeth

and it is evident that 2nd teeth have a combination of colors, green, light green, and blue which ensures that flux linkage of this teeth is comparatively less than the 1st teeth reason because the distance of 2nd teeth from the magnet is comparatively greater than 1st teeth. That's the reason the magnet does not get attracted toward 2nd teeth in the absence of the magnetic field of the coil.

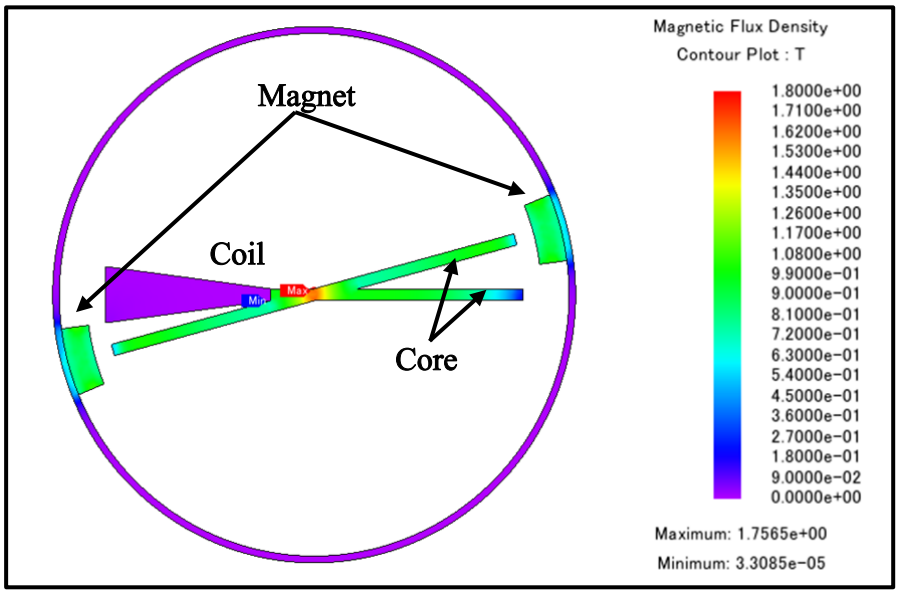

Figure 19: Simulation Result of Magnetic Field Interaction Between Magnet, Coil, and Core Teeth Without Current Passage

The next case is the energization of the coils on the 2nd teeth by the current. The current flowing through the coil will produce its magnetic field and the magnet will be attracted by the magnetic field of the coil and align itself with the 2nd teeth. The magnet and current-carrying coils are oriented in such a way that attractional force will be the result of the interaction of magnetic fields instead of the repulsion. Because attraction is the controlled pattern of rotation. The magnet will not force the rotor to move to 3rd coil if it is attracted by the 2nd coil. The simulation is done only for one set of teeth and coil attraction, The same phenomenon will be repeated between 3rd and 2nd coil, 4th and 3rd

coil, 5th and 4th coil, 6th and 5th coil. Based on these simulation results when the winded actuator is tested, it worked perfectly fine. Figure 20 will show the result of the current passage through 2nd coil, and the resulting rotation of the permanent magnet by a step angle of 15 degrees.

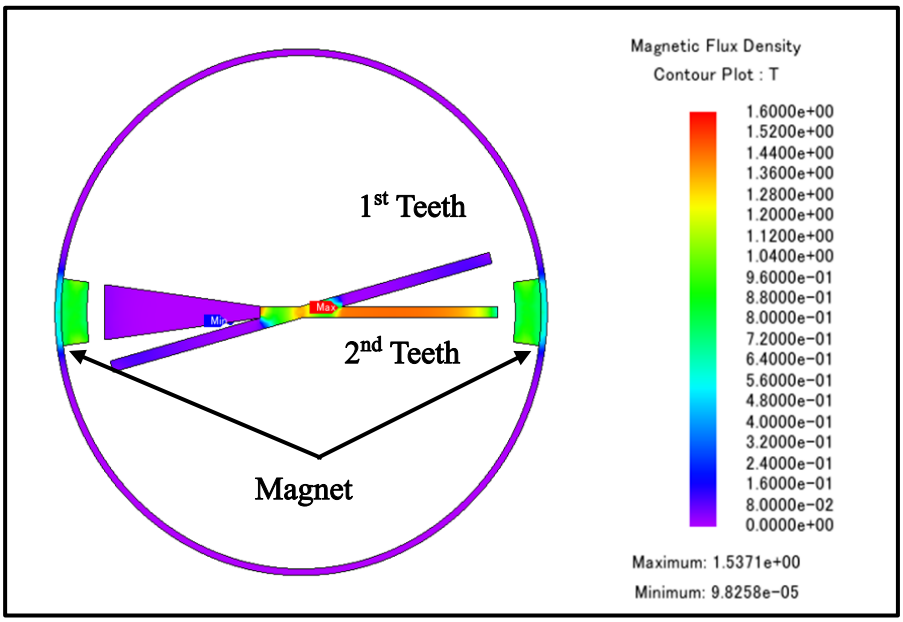

Figure 20: Simulation Result of Magnetic Field Interaction Between Magnet, Coil, and Core Teeth Due to Passage of Current Passage

Figure 20 shows that the permanent magnet is now facing the 2nd teeth instead of the 1st teeth. The coil is removed intentionally from the one end of the 2nd teeth to see the pattern of magnet flux density linkage. The major contribution of color on the 2nd teeth is orange and the minor contribution is of green color. Whereas the color on the 1st teeth has turned to bluish-purple, the reason is because the permanent has moved to 2nd teeth from the 1st teeth. Now almost all of the magnetic field lines of the permanent magnets are passing from one end of the 1st magnet to the other end of the 2nd magnet through the core because the opposite poles of both magnets are facing each other. Figure 21

shows the isometric view of the simulation in Figure 19 to show the flux linkage of the ends of the magnets which are facing each other.

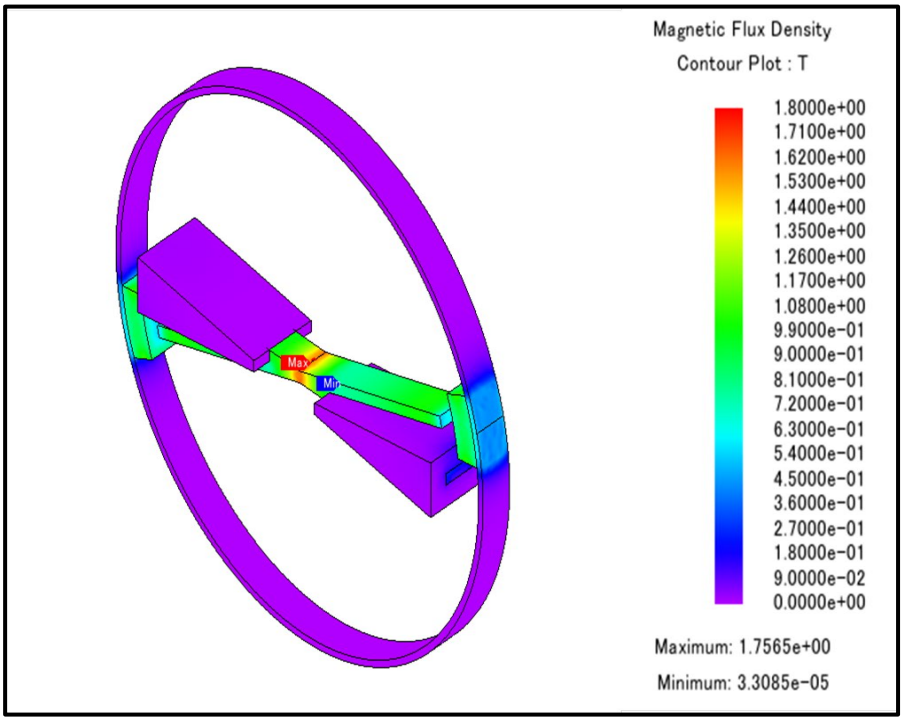

Figure 21: Isometric view of Simulation Result of Magnetic Field Interaction Between Magnet, and Core Teeth

IMPROVEMENT AFTER STEPPING ACTUATOR DESIGNING

The improvements made by the motor's redesign are significant, producing important advancements:

SPACE EFFICIENCY

From 30 degrees to 15 degrees, the angle between adjacent coils was half. Six coils might be integrated into the same physical area that originally held four thanks to space optimization. This increase in coil count resulted in a wider variety of flow-setting levels, which improved system flexibility.

VOLTAGE EFFICIENCY

The newly created micro-stepping actuator drives the same load efficiently at 5 V while utilizing a smaller power source. This is a remarkable reduction in power use without a drop in quality. The suggested design uses silicon tubing to create an outside boundary that unites the actuator, valve, and mechanism for collecting the discharged liquid. The benefit of this thorough design strategy is that it guarantees that hydrostatic variances caused by elements like silicon tubing or fluctuations in liquid levels inside the reservoir will not negatively impact system performance during testing. A system design that is simplified and reliable is encouraged by this degree of integration.

CEREBROSPINAL DYNAMICS

The current entering node as shown in Figure 22 represents the formation of CSF and the current leaving that same node and flowing into the branch showing a capacitor in it represents the CSF storage and the current flowing into the branch having diode indicates the resistance faced by it and diode indicates the unidirectional flow of the current. According to the current conservation law, the sum of currents flowing into the node should be equal to the current flowing out of the node. CSF production should be balanced by reabsorption and storage for the equilibrium of the CSF dynamic state.

$$\text{CSF Production}(I_P) = \text{CSF Storage} + \text{CSF Reabsorption}(I_R) \quad \text{.....eq.(22)}$$

I_R is a differential of potentials divided by the resistance to CSF outflow (R_{CSF}).

$$I_R = \frac{P(t) - P_{SS}}{R_{CSF}} \quad \text{.....eq.(23)}$$

P_{SS} normal value lies between 3 and 10 mmHg[35]. The opposition to CSF reabsorption is known as (R_{CSF}) and has units (mm Hg/(mL/min)). The compliance of the cerebrospinal fluid space (C), measured in [mL/mm Hg], is inversely related to the

differential pressure and capacity of storage based on the capability of the skull to store a certain volume.

$$I_S = C\frac{dp}{dt} \quad \text{.....eq.(24)}$$

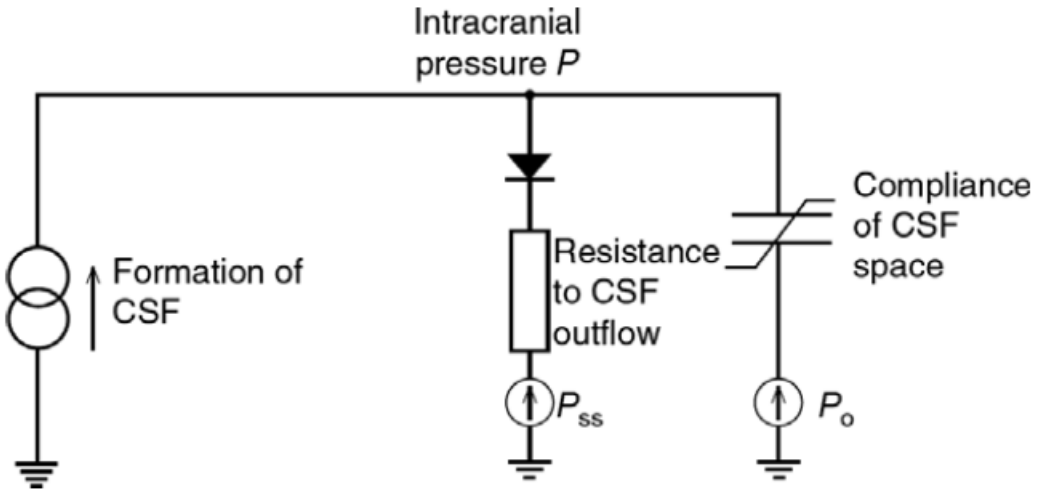

Figure-22: Electrical Representation of CSF Dynamics

VALVE SEAT DESIGNING

An essential component of the ball-in-cone valve's functioning that has significant significance for flow rate control is the painstaking construction of the ball seat. A thorough strategy was used to solve this crucial component, which included using a resin printer to create several cone shapes. The precise design of these made-to-order cones allows for a variety of seat contact angles, including 35, 40, 45, 50, 55, 60, and 65 degrees. The ensuing annular clearance, which serves as the authorized channel for fluid flow, is largely determined by the contact angle that the ball and the cone share. The relative movement of the ball, prompted by changes in intracranial pressure, or the plunger's activation all have an inherent effect on this dynamic clearance. Therefore, the seat design is of utmost importance in precisely controlling fluid flow inside the ball-in-cone valve, indicating its crucial role in the system's operational performance. In the comprehensive testing of different cone arrangements, it was found that using a seat contact angle of 65 degrees resulted in the best flow rate controllability. It became very difficult to lower the flow rate to zero or almost zero levels after the cone was forced away from the seat by the force of the incoming fluid, a problem that persisted across all tested cones. The fundamental purpose of the ball-in-cone valve seat, which is to accurately modify flow rates by adjusting to changes in annular space between the cone and ball, was severely hampered by this inconsistency. An original strategy was used to overcome this inherent constraint and guarantee a reliable seal inside the cone seat profile. When the stainless-steel ball was heated and placed within the resin cone, a

unique interaction was created between the ball and the interior surface of the cone. By smoothly adjusting the cone's internal geometry, the ball was able to effectively reflect the curvature of its spherical form. The difficulty of maintaining a constant and dependable seal within the ball-in-cone valve was effectively solved by this clever technique, which improved flow rate control. The ability of this redesigned cone arrangement to successfully lower the flow rate to almost nothing when the ball contacted the seat profile was significantly improved after thorough testing. This distinctive characteristic, which is an indication of effective flow rate control, was a crucial realization throughout the iterative design process for the cone form. To achieve the best seal and flow modulation, the main goal changed to minimizing the clearance space between the ball and the cone seat profile when they make contact. It's significant to notice that the rate of CSF flow is significantly influenced by the clearance area of the annular space. The velocity of the flow increases in direct proportion to the clearance area of the annular gap, which corresponds to an increase in clearance between the ball and cone. The perfect management of cerebrospinal fluid flow depends heavily on this direct correlation between annular spacing and flow rate. Additionally, the flow rate's interaction with resistance is directly influenced by the cone angle. A bigger cone angle provides more space for the ball's curve to interact with the cone seat profile. Because of the greater resistance to incoming fluid created by this structure, it takes more energy to compress the spring at the inlet, thereby increasing the ball's opening pressure. Cone angle, resistance, and opening pressure have an innate connection that is crucial for optimizing the valve's performance characteristics. This configuration, which includes a secondary cone, makes a major contribution to the

regulation of the flow rate within the apparatus. The impact of the entering has an effect, on the primary cone, located on the inlet or closer side compared to its influence on the secondary cone, which operates differently. The motion of the ball in the cone is primarily caused by the pressure exerted by the fluid. It's important to note that as pressure increases there is an increase in clearance between the ball and cone seat leading to higher flow rates. The second cone, positioned in the direction of the one serves a distinct purpose in response to changes, in fluid pressure. The second cone approaches the bottom of the first cone as the pressure of the entering fluid increases. The action of the plunger also simultaneously lifts the ball within the second cone. This carefully planned interplay between the plunger, ball, and cone enables accurate flow control. The back-and-forth action of the plunger is closely related to the radius of the ball. The radius of the ball within the cone and the hemispherical cam's maximum vertical height are the same. This size gives the plunger the most room to move within the cone seat, allowing it to effectively raise or lower the ball to change the flow rate as needed. To achieve proper flow control and keep the system functioning, these complex mechanical interactions are necessary. The hemispherical cam's height gradually decreases as part of the system's control mechanism, going from its greatest height to zero height throughout six stages that cover 90 degrees of rotation. The hemispherical cam aligns concentrically with the rotor's diameter at zero height. Controlled testing, which comprised adjusting the fluid level in the tank in increments of microliters, was used to evaluate the valve's performance and reactivity to shifting circumstances. The microcontroller delays, responsiveness of the flow sensor, fluidic resistances, and mechanical oscillations caused by the plunger's motions and spring compressions and

expansions were all considered by this exact measurement technique. Due to its extraordinary resistance to corrosion and biocompatibility, titanium was selected for the construction of the cone, guaranteeing its appropriateness for this medical equipment. Integrated into the proximal end of the first cone is a spring with a 7.29 N/m spring constant. About 2.43 mN of force is required to dislodge the ball away from the cone seat profile and start the fluid flow. A vertical titanium column is incorporated with the cone seat contour to preserve the ball's concentric location within the cone. The ball's movement is successfully constrained by this configuration, keeping it in line with the cone. Fluid flow encounters resistance when the portion of the cone seat profile in touch with the ball is used, and this is referred to as "R_{Start}." Following that, when the ball deviates from the cone seat profile, the fluid flow faces resistance from the vertical column, known as "R_{Side}." As long as, the ball is concentric with the cone, the vertical column's resistance does not change, helping to control fluid flow, especially while switching from turbulent to laminar flow. Variability may be seen in the resistance shown by "R_{Side}." when the ball is not in a concentric position. According to the continuity equation's basic tenet, the amount of fluid flowing per second is represented by the area times the fluid velocity at different cross-sectional sites across the pipe. More broadly, it might be said that there is no change in velocity overall. The Navier-Stokes equation, for the analysis of incompressible fluids, is an excellent tool to get a thorough grasp of the fluid mechanics involved. The cone, spring, and supports, together with the other resistance elements, all work together to cause the device to behave passively. Variations in the flow rate (Q) are significantly influenced by this

passive characteristic. The following is the expression for the Hagen-Poiseuille equation, which is used to determine flow in annular areas.

$$Q = \frac{\Delta P \times \pi (R_o{}^2 - R_i{}^2)}{8\mu L} \left[(R_o{}^2 - R_i{}^2) - \frac{(R_o{}^2 - R_i{}^2)}{\ln\left(\frac{R_o}{R_i}\right)} \right] \text{.....eq.(25)}$$

The radii of the annular areas, with R_o denoting the outer radius and R_i denoting the inner radius of the annular zone, regulate the Hagen-Poiseuille equation. In this equation, pressure fluctuation and flow rate have a direct connection, but the resistive length of the fluidic channel shows an inverse relationship. It becomes clear that increasing flow rates are correlated with bigger pressure fluctuations and disparities between annular zone radii.

MANUAL TESTING OF SHUNT DEVICE

To avoid any possible leakage of nano-filtered water, epoxy was strategically applied at the joints during the installation of all the parts of the proposed shunt mechanism. This decision was made based on how closely the chemical and physical characteristics of nano-purified water matched those of cerebrospinal fluid (CSF). The epoxy performed a dual function by protecting the teeth of the micro stepping actuator from direct contact with nano-filtered water and also serving as an insulator for them. Specific safety measures were adopted since the micro-stepping actuator is situated inside the water's flow route. The actuator included six separate coils, each of which was attached to a different electrical line that served as a control pin. The actuator's rotor began to rotate when these coils were activated, and this caused the stainless-steel ball to move around in the second cone, adjusting the flow rate to the desired level. To evaluate the flow rate responses of this shunt device with cmH_2O and at different valve settings, it underwent extensive manual testing. For a clear illustration of the variations in flow rate under various pressure and valve settings, visual representations in the form of figures were used.

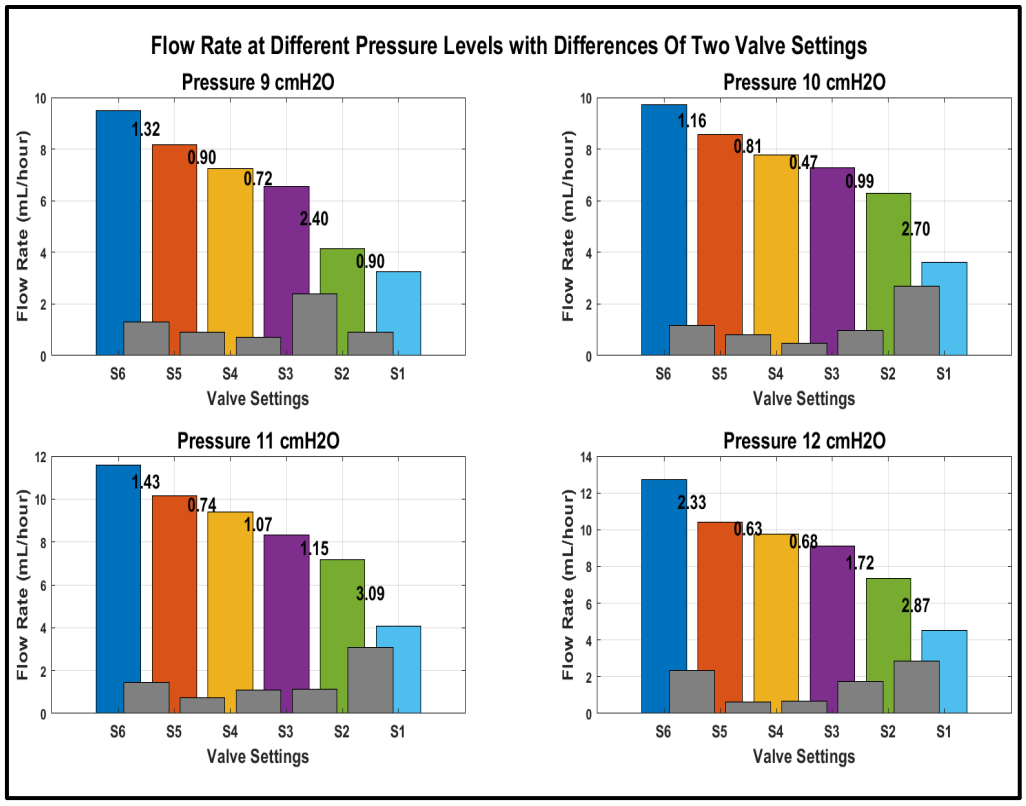

Figure 23: Manual Testing of Shunt Device Various Pressure and Valve Setting

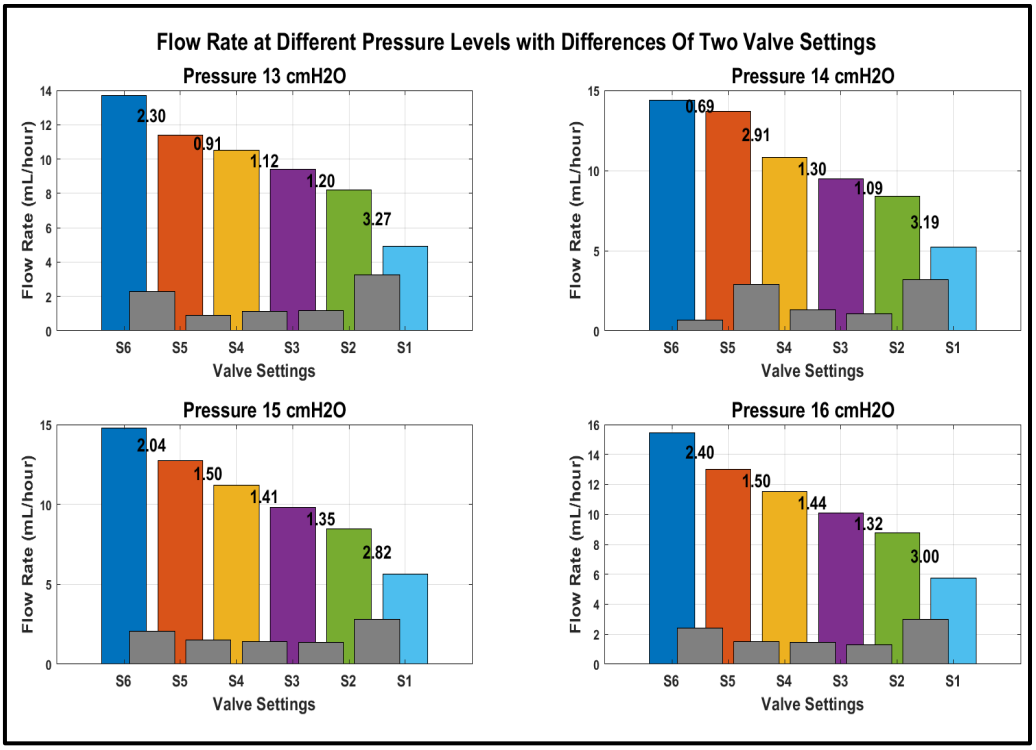

Figure 24: Manual Testing of Shunt Device Various Pressure and Valve Setting

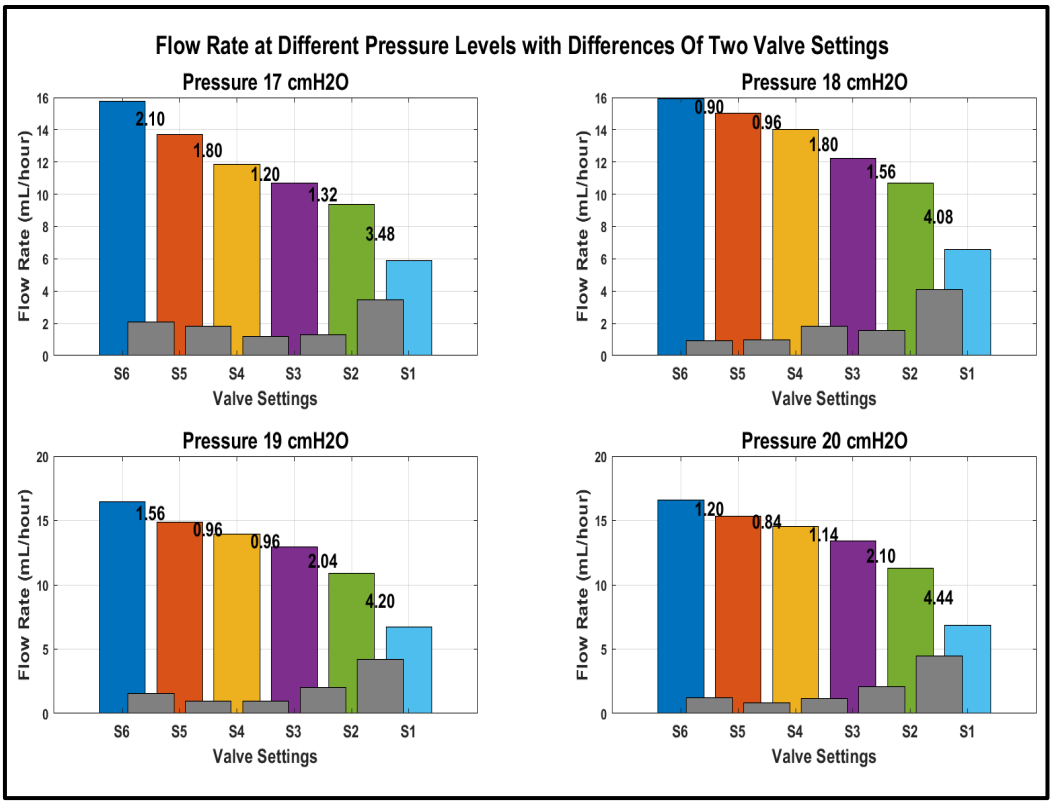

Figure 25: Manual Testing of Shunt Device Various Pressure and Valve Setting

Manual flow rate tests within a particular pressure range were part of the assessment procedure. The pressure was manually increased by adding water to the graduated cylinder, starting at 10 cmH_2O with the valve completely open and a flow rate of 9.78 mL/hr. The observed variations in flow rate offered insightful information. The flow rate increased from 9.78 mL per Hour to 10.68 mL per Hour when the pressure rose from 10 to 11 cmH_2O. The flow rate dropped to 9.18 mL per Hour while keeping the pressure at 11 cmH_2O after manually activating the coil causing the ball within the cone to slide closer to the bottom of the seat and reduce the clearance space. We made some adjustments, to the pressure during the procedure. When we increased the pressure from 11 to 12 cmH2O we noticed an increase in the flow rate from 9.18 to 11.16 mL per hour.

It's important to mention that when we manually activated the coil at a pressure of 12 cmH2O the flow rate went down to 9.18 mL per hour. We made changes. Decided to raise the pressure from 12 to 13 cmH2O. Consequently the flow rate increased from 9.48 to 10.32 mL per hour. However when we turned on the coil while maintaining a pressure of 13 cmH2O the flow rate decreased from 10.32 mL per hour to 7.92 mL per hour. Finally as we increased the pressure again from 13 to 14 cmH2O there was another increase in flow rate from 7.92 mL per hour up to 8.58 mL, per hour. To better understand these observations please refer to the accompanying graph.

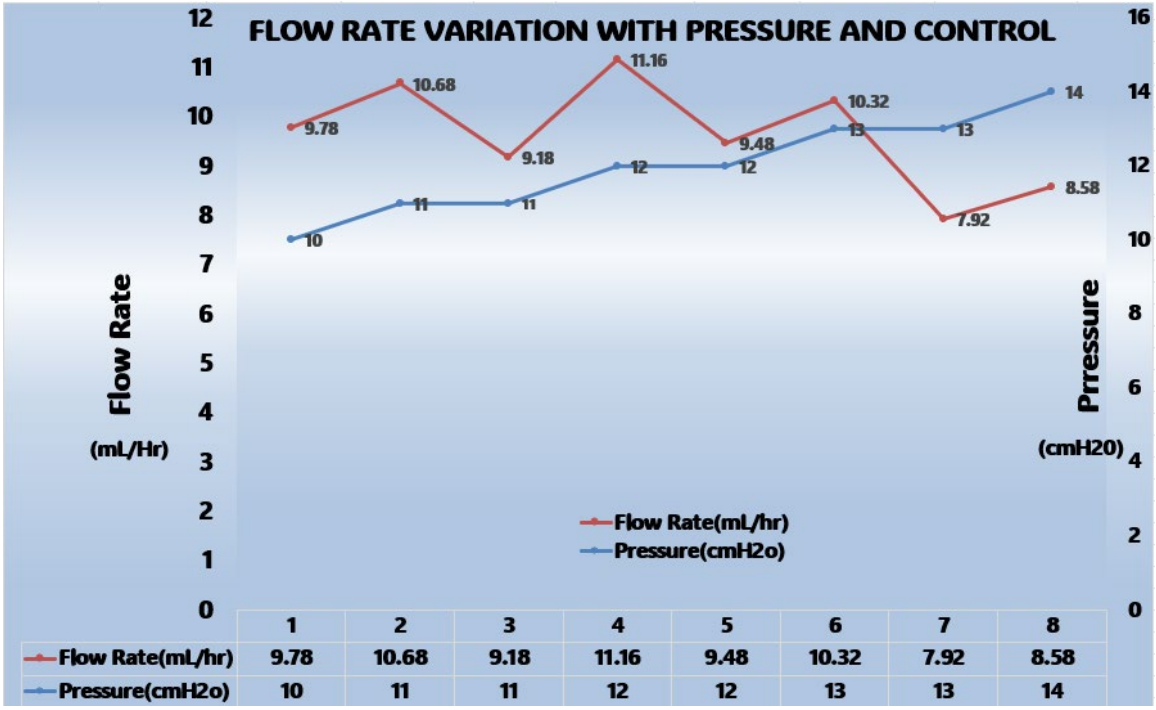

	1	2	3	4	5	6	7	8
Flow Rate(mL/hr)	9.78	10.68	9.18	11.16	9.48	10.32	7.92	8.58
Pressure(cmH2o)	10	11	11	12	12	13	13	14

Figure 26: Manual Testing of Shunt Device From pressure 10 to 14 cmH_2O

AUTOMATIC TESTING OF SHUNT DEVICE

An ongoing flow rate spike that caused a sudden rise before leveling out at its real value was discovered during the automated testing of the shunt device. Due to this surge, the microcontroller received a false-positive indication about the flow rate. The system mistakenly followed the false positive signal rather than stabilizing at the appropriate number. A thorough investigation established that the shock the rotor felt while rotating was the cause of the flow rate surge. Two magnetic fields—one produced by the magnet and the other by the coil when it was charged by the flow of current—interacted to cause this jolt. The bearing, which is attached to the rotor and pivots with the assembly's central shaft, was altered to remedy this problem by having its diameter increased. With this modification, the jerk was greatly reduced, which helped to reduce the flow rate rise during testing. The area of the hemispherical cam height where there was no plunger displacement was where the jerk intensity was most noticeable. The intensity of these oscillations decreased as the hemispherical cam's thickness rose, which in turn compressed the spring. Technically speaking, it may be considered that the spike intensity increases while the mini-stepping actuator is empty and drops when the actuator experiences loading. Another strategy, including lowering the excitation voltage provided to the mini-stepping actuator, was used to further reduce the jerk's intensity. The jerk intensity was successfully reduced by this change when the gadget was in use. A comprehensive analysis led to the conclusion that 3 volts was the ideal excitation voltage. The device was found to operate at this voltage effectively at full

load circumstances, guaranteeing stability in flow control, especially at thicker hemispherical cams. A careful analysis of the device's operating characteristics was conducted, accounting for elements including microcontroller feedback delays, frictional forces, and mechanical oscillations. The flow rate varied, often within a range of 2 to 3 mL per Hour and sometimes led to under- or over-drainage at higher speeds or when the stepping actuator is not loaded. During testing, this diversity was carefully observed and assessed.

MOTIVATION BEHIND THE CUSTOMIZED DESIGNNG OF ACTUATOR

There were two reasons for creating a unique motor. First, it sought to perfectly match the actuation specifications of our design with the physical parameters of the shunt prototype. To achieve a small design, it also aimed to decrease power consumption and lessen the dependency on electrical components. The majority of commercially available stepper and micro servo motors need extra control circuitry to regulate speed and step, posing size and component use limitations. Eliminating extraneous parts that didn't fit the requirements of our design was our aim. A comparison of existing stepper motors and our created micro-stepping actuator can be seen in the table below:

Product Name	**Stepper Motor SM3.7-20**	**Stepping Actuator**
No. of Steps (step angle)	20 (1 Step Angle = 18)	24 (1 Step Angle = 15)
Coil Resistance	22 ohm/phase	44 ohms
Pull-In Torque	0.045 m N-m	2.2 m N-m

Table 2: Comparison of Torque Produced and Step Angle [36]

When compared to the smallest commercially available stepper motors, the developed micro stepping actuator exhibits several significant benefits in this comparative

examination. These benefits directly affect how well our shunt device's ball-in-cone flow control mechanism works to manage flow rates. First off, compared to the smallest available stepper motor, the developed micro-stepping actuator provides a much-reduced step size. When regulating the flow rate using the ball-in-cone mechanism, the finer granularity of the step size offers more accuracy and control. Second, by a wide margin, the torque produced by the proposed micro-stepping actuator exceeds that of the smallest stepper motor. For our needs, this increased torque is very important since it is essential for compressing the spring and adjusting the clearance width between the annular areas of the cone to control fluid flow. The main problem with commercially accessible motors, particularly smaller ones, is that size, speed, and torque are always traded off. Our fundamental need for precise torque to regulate fluid flow via the cone valve does not correspond with smaller motors' tendency to provide faster speeds but less torque. By offering improved step size and torque characteristics, the developed micro stepping actuator successfully solves this restriction, making it a good fit for our application. A flow sensor, an Arduino Nano microprocessor, and a display unit for real-time flow rate measurements are all integrated into the designed shunt device. Together, these parts provide effective monitoring and management of the shunt device's operation. The flow sensor is essential to this system because it measures flow rates precisely and sends that information to the microcontroller via the I_2C interface, which offers a high 16-bit resolution for accuracy. The developed small stepping actuator has a maximum current flow requirement of 500 mA, albeit it operates at its best at 300 mA. A 5V external power source is used to power the complete system. It's vital to remember that the 40-mA current supply capability of the Arduino Nano microcontroller's digital pins is inadequate

for managing the coil energizing current needs. Transistors are included into the circuit to efficiently regulate and control the current flow to the motor pins to get around this restriction. When six coils electrical connecting cables link to the microcontroller, and when required, these connection points may also operate as a manual override method for coil activation. With the help of this adaptable system, the shunt device may be powered effectively, and all its many parts works together to accomplish the appropriate flow control and monitoring goals.

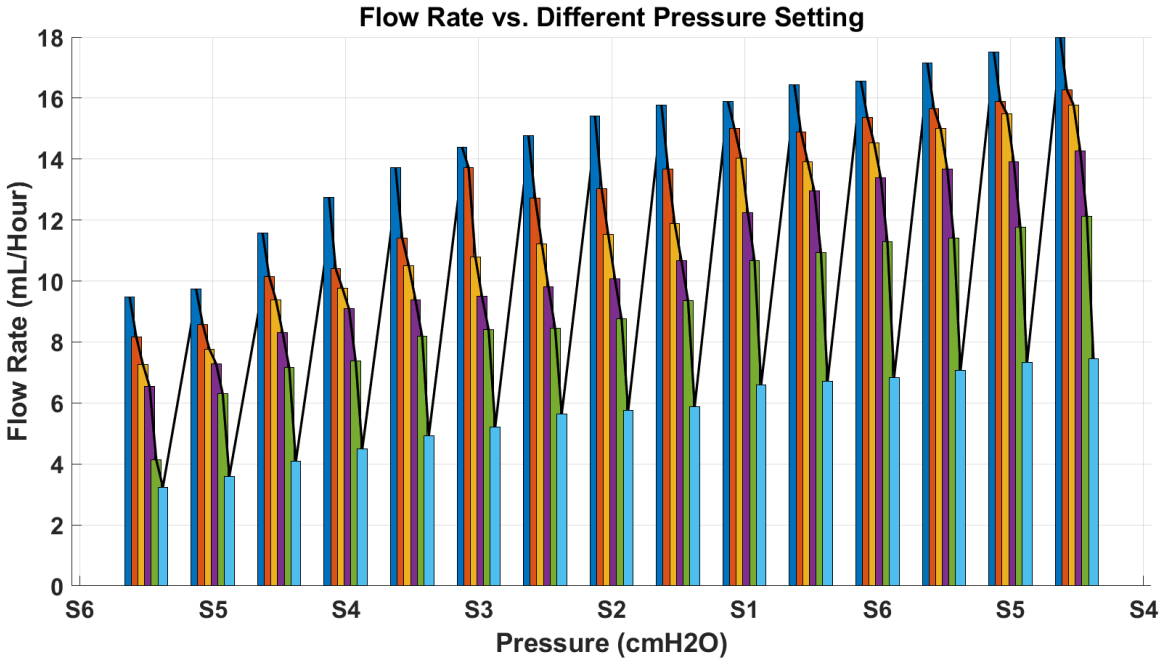

Figure 27: Automatic Testing of Shunt Device From pressure 10 to 14 cmH_2O

EFFECT OF POSITIONAL CHANGE

The shunt device underwent several orientation adjustments during testing, including being positioned vertically. The device's operation was impacted by this orientation change in several ways. The gravitational force (W = mg) acting on the stainless-steel ball within the first cone increased the permissible area for fluid flow at the intake of the

first cone when it was positioned vertically. It also squeezed the cone's accompanying spring at the same time. As a result of the change in orientation, the gravitational force also had an impact on the ball within the second cone, reducing the area that could be used for fluid flow. This produced a unique situation in which the device's change in location had opposing impacts on the regulation of flow in the two cones. Contrary to original assumptions, the flow rate did not noticeably change because of the device's orientation adjustment. This discovery suggested that the second cone had two functions: it was a stop valve and a flow regulator. The device continued to carry out its intended tasks despite changes in orientation because it efficiently prevented backflow in situations when there was a pressure decrease at the intake.

FUTURE WORK, DISCUSSION AND CONCLUSION

The designed shunt device has undergone promising testing, and consequently, is well-positioned as a powerful prototype for efficient flow control over a range of pressure changes. These findings imply that this prototype, if approved, has the potential to stand out as an original approach among other shunt devices, especially given its suitability as an external ventricular drainage (EVD) device. This gadget's design has been thoughtfully crafted with a focus on its potential as an implanted device, minimum power consumption, small dimensions to guarantee efficient performance, and external connectivity possibilities. To do this, the design process placed a strong emphasis on lowering the device's reliance on sensors and electronics while retaining its functionality. The important knowledge and information gained during this study is anticipated to be used as a crucial basis for the creation of more sophisticated designs that satisfy the exacting standards for implanted devices that have received clinical approval. Any automated flow control shunt device must have an actuator, which became clear during the development process. By effectively converting electrical energy into mechanical energy, this actuator plays a crucial part in enabling changes in flow control. The difficulty increases as the device becomes smaller, highlighting how difficult it is to manage flow in small-footprint devices. These results suggest an encouraging path for the development of medical technology and better patient care. It becomes clear that using pre-made off-the-shelf actuators is not the best choice when looking for highly effective and small-footprint automated flow control solutions. This unique actuator design enables

exact customization of the device's operation to meet the necessary requirements. This provides the opportunity to further scale down the device's size and increase its overall compactness. The sensitivity of the flow rate to elements like head motions or vibrations has also come into play throughout the development of these systems, necessitating the inclusion of these impacts in the design. Recognizing the constraints involved with continuous active control, including the possibility for increased battery consumption, a more realistic strategy is to specify a range for flow control rather than concentrating entirely on obtaining a given flow rate number. This strategy maintains the device's useful functionality while maximizing its operating longevity. The produced micro stepping actuator's design still has space for development, since several design details that maximize size reduction were not originally obvious during the actuator's initial design. These modifications could reduce the system's size by half, highlighting the room for improvement and creativity in the search for smaller, more effective gadgets. Currently, the system's small stepping actuator, which has six coils spread at 15-degree intervals, takes up half of the 360-degree area. By increasing the number of coils by two, there is a chance for considerable improvement. This enlargement would entail fitting a total of 12 coils into the available 180-degree area. This improvement would result in enhanced control valve capabilities, allowing for even more accurate flow management. The size of the ball used in the control valve has an inherent relationship with its performance. A bigger operational area for fine-tuning flow control is made available by using a larger ball with an expanded radius, making it a crucial factor for optimization. It also offers promise for optimizing the device's functioning to use wireless power transfer. A more sophisticated and self-sufficient system may be made by incorporating wireless

communication for the control valve and the tiny stepping actuator, as well as a rechargeable battery that is covertly implanted under the skull. The microcontroller and other electrical components required for active monitoring and control would need to be wearable or pocket-sized under this strategy. While retaining device functioning, this setup may make things easier to use and more convenient.

CODE

Source Code For Solution of Design Equation For Mini Stepping Actuator:

```
%% Initial Sizing of stepping machine
clear; clc; close all;
Pout    = 0.0012;                % (kW) desired output Power
w_rpm     = 5000;                % (rpm) rated speed
w_rps   = w_rpm/60;              % (rps) rated speed
w       = w_rpm*2*pi/60;         % (rad/sec) rated speed
Efficiency    = 0.48;            % desired efficiency
Vdc     = 5;                     % (V) input DC voltage
m       = 1;                     % (no.) no. of phases
Pin     = Pout/Efficiency;       % (kW) input power
It      = Pin*1000/Vdc;       % (A) average terminal current (from DC source)
Torque  = Pout*1000/w;           % (Nm)
Np      = 1;                    % (no.) number of parallel paths in winding
Iph_pk  = It;                   % (A) peak value of phase current
Iph_rms = (sqrt(2/3))*Iph_pk;  % (A) rms value of phase current
Ic_pk   = Iph_pk/Np;            % (A) rms value of coil current
% Ic_rms  = Iph_rms/Np;         % (A) rms value of coil current
%% Volumetric Parametrization
tau     = 0.0869;               % aspet ratio of machine (Tau = l/D)
kw      = 0.95;                 % winding factor
Bav     = 0.7;                  % (T) magnetic loading
As      = 3.8e4;                % (A/m) electric loading
```

```
Span    = 90;                   % (deg) span of the whole motion
Steps   = 6;                    % (nos.) no. of steps in whole span of motion
Theta   = Span / Steps;         % (deg) angle for single step
Theta_m = Theta * pi/180;       % (rad) angle for single step
% l1 = 0.004
% D1 = 0.046
% Ntph1 = 460
% I_coil1 = 0.5
% As1 = 2*m*Ntph1*I_coil1/(D1*theta_m)
T1 = ( (1/(2*pi)) * kw * Bav * As * (D1^2) * (theta_m^2) * l1 )
D       = round ((Torque/((tau/(2*pi))*kw*Bav*As*(Theta_m^2)))^(1/3),3);
% (m) airgap diameter of the machine
l       = tau * D;              % (m) stack length of machine
Ns      = 2;                    % (nos.) no. of stator teeth
Ntph    = ( As * D * Theta_m ) / (2 * m * Ic_pk);
% (nos.) no. of turns per phase
Ntc     = m * Ntph / Ns;        % (nos.) no. of turns per coil
%% Magnet Dimensions
mu_r    = 1.05;                 % recoil permeability of magnet N52
g       = 0.002;                % (m) airgap
kr      = 1.1;                  % reluctance factor
kl      = 0.9;                  % leakage factor
Br      = 1.40;                 % (T) remanent flux density of magnet N52
C_phi   = 1;                    % concentration factor (Am/Ag)
L_pm    = (mu_r * Bav * g * kr) / ((kl*Br) - (Bav/C_phi));
                        % (m) length of permanent magnet
%                     alpha_p                     =                     0.9;
% ratio of magnet arc to magnetic-pole arc
```

```
Nm      = 2;                    % no. of magnets (rotor poles)

w_m     = (D/2) * Theta_m;      % (m) average width of permanent magnet

% magnetic loading reverse calculation

% lpm  = 0.003

% Bav1 = (lpm * kl * Br) / ((mu_r*g*kr) + (lpm/C_phi))
```

REFERENCES

[1] H. L. Rekate, “A Contemporary Definition and Classification of Hydrocephalus,” *Semin Pediatr Neurol*, vol. 16, no. 1, pp. 9–15, Mar. 2009, doi: 10.1016/J.SPEN.2009.01.002.

[2] R. Spector, S. Robert Snodgrass, and C. E. Johanson, “A balanced view of the cerebrospinal fluid composition and functions: Focus on adult humans,” *Exp Neurol*, vol. 273, pp. 57–68, Nov. 2015, doi: 10.1016/J.EXPNEUROL.2015.07.027.

[3] L. Sakka, G. Coll, and J. Chazal, “Anatomy and physiology of cerebrospinal fluid,” *Eur Ann Otorhinolaryngol Head Neck Dis*, vol. 128, no. 6, pp. 309–316, 2011, doi: 10.1016/J.ANORL.2011.03.002.

[4] M. Bergsneider, C. Miller, P. M. Vespa, and X. Hu, “Surgical management of adult hydrocephalus,” *Neurosurgery*, vol. 62 Suppl 2, no. SUPPL. 2, Feb. 2008, doi: 10.1227/01.NEU.0000316269.82467.F7.

[5] J. Inamasu *et al.*, “Postoperative communicating hydrocephalus in patients with supratentorial malignant glioma,” *Clin Neurol Neurosurg*, vol. 106, no. 1, pp. 9–15, 2003, doi: 10.1016/S0303-8467(03)00060-X.

[6] F. NIGIM, J. F. CRITCHLOW, and E. M. KASPER, “Role of ventriculoperitoneal shunting in patients with neoplasms of the central nervous system: An analysis of 59 cases,” *Mol Clin Oncol*, vol. 3, no. 6, pp. 1381–1386, Nov. 2015, doi: 10.3892/MCO.2015.627.

[7] J. Roth, S. Constantini, D. T. Blumenthal, and Z. Ram, “The value of ventriculo-peritoneal shunting in patients with glioblastoma multiforme and ventriculomegaly,” *Acta Neurochir (Wien)*, vol. 150, no. 1, pp. 41–46, Jan. 2008, doi: 10.1007/S00701-007-1454-0.

[8] F. Khan, A. Rehman, M. S. Shamim, and M. E. Bari, “Ventriculoperitoneal (VP) Shunt Survival in Patients Developing Hydrocephalus After Cranial Surgery,” *Turk Neurosurg*, vol. 26, no. 3, pp. 369–377, 2016, doi: 10.5137/1019-5149.JTN.11447-14.1.

[9] “Ventricles of the Brain | Structure, Functions & Uses - Video & Lesson Transcript | Study.com.” Accessed: Oct. 19, 2023. [Online]. Available: https://study.com/learn/lesson/ventricles-of-the-brain.html

[10] P. D. Brown, S. L. Davies, T. Speake, and I. D. Millar, “Molecular mechanisms of cerebrospinal fluid production,” *Neuroscience*, vol. 129, no. 4, pp. 955–968, Jan. 2004, doi: 10.1016/J.NEUROSCIENCE.2004.07.003.

[11] H. Reiber, “Flow rate of cerebrospinal fluid (CSF) - A concept common to normal blood-CSF barrier function and to dysfunction in neurological diseases,” *J Neurol Sci*, vol. 122, no. 2, pp. 189–203, 1994, doi: 10.1016/0022-510X(94)90298-4.

[12] T. H. Milhorat, “The third circulation revisited,” *J Neurosurg*, vol. 42, no. 6, pp. 628–645, Jun. 1975, doi: 10.3171/JNS.1975.42.6.0628.

[13] M. Edsbagge, M. Tisell, L. Jacobsson, and C. Wikkelso, “Spinal CSF absorption in healthy individuals,” *Am J Physiol Regul Integr Comp*

Physiol, vol. 287, pp. 1450–1455, 2004, doi: 10.1152/ajpregu.00215.2004.-The.

[14] "Subcommissural organ, cerebrospinal fluid circulation, and hydrocephalus | Semantic Scholar." Accessed: Oct. 19, 2023. [Online]. Available: https://www.semanticscholar.org/paper/Subcommissural-organ%2C-cerebrospinal-fluid-and-P%C3%A9rez-F%C3%ADgares-Jim%C3%A9nez/7a4321f06c3a03d25149fff0c59c8eaece773338

[15] C. May, J. A. Kaye, J. R. Atack, M. B. Schapiro, R. P. Friedland, and S. I. Rapoport, "Cerebrospinal fluid production is reduced in healthy aging," *Neurology*, vol. 40, no. 3 Pt 1, pp. 500–503, 1990, doi: 10.1212/WNL.40.3_PART_1.500.

[16] R. O. Weller, E. Djuanda, H. Y. Yow, and R. O. Carare, "Lymphatic drainage of the brain and the pathophysiology of neurological disease," *Acta Neuropathol*, vol. 117, no. 1, pp. 1–14, 2009, doi: 10.1007/S00401-008-0457-0.

[17] S. Gupta, M. Soellinger, P. Boesiger, D. Poulikakos, and V. Kurtcuoglu, "Three-dimensional computational modeling of subject-specific cerebrospinal fluid flow in the subarachnoid space," *J Biomech Eng*, vol. 131, no. 2, Feb. 2009, doi: 10.1115/1.3005171.

[18] J. D. Miller, D. P. Becker, J. D. Ward, H. G. Sullivan, W. E. Adams, and M. J. Rosner, "Significance of intracranial hypertension in severe head injury," *J Neurosurg*, vol. 47, no. 4, pp. 503–516, Oct. 1977, doi: 10.3171/JNS.1977.47.4.0503.

[19] M. Czosnyka and J. D. Pickard, “Monitoring and interpretation of intracranial pressure,” *J Neurol Neurosurg Psychiatry*, vol. 75, no. 6, pp. 813–821, Jun. 2004, doi: 10.1136/JNNP.2003.033126.

[20] A. J. W. Boon *et al.*, “Dutch normal-pressure hydrocephalus study: prediction of outcome after shunting by resistance to outflow of cerebrospinal fluid,” *J Neurosurg*, vol. 87, no. 5, pp. 687–693, 1997, doi: 10.3171/JNS.1997.87.5.0687.

[21] R. Katzman and F. Hussey, “A simple constant-infusion manometric test for measurement of CSF absorption. I. Rationale and method,” *Neurology*, vol. 20, no. 6, pp. 534–544, 1970, doi: 10.1212/WNL.20.6.534.

[22] A. Behrens, N. Lenfeldt, S. Qvarlander, L. O. Koskinen, J. Malm, and A. Eklund, “Are intracranial pressure wave amplitudes measurable through lumbar puncture?,” *Acta Neurol Scand*, vol. 127, no. 4, pp. 233–241, Apr. 2013, doi: 10.1111/J.1600-0404.2012.01701.X.

[23] H. Stephensen *et al.*, “There is no transmantle pressure gradient in communicating or noncommunicating hydrocephalus,” *Neurosurgery*, vol. 50, no. 4, pp. 763–773, Apr. 2002, doi: 10.1097/00006123-200204000-00016.

[24] R. Taylor, Z. Czosnyka, M. Czosnyka, and J. D. Pickard, “A laboratory model of testing shunt performance after implantation,” *Br J Neurosurg*, vol. 16, no. 1, pp. 30–35, 2002, doi: 10.1080/02688690120114200.

[25] A. Aschoff, “In-Depth View: Functional Characteristics of CSF Shunt Devices (Pros and Cons),” *Textbook of Pediatric Neurosurgery*, pp. 1–40, 2019, doi: 10.1007/978-3-319-31512-6_26-2.

[26] T. Yasuda, T. Tomita, D. G. McLone, and M. Donovan, “Measurement of cerebrospinal fluid output through external ventricular drainage in one hundred infants and children: correlation with cerebrospinal fluid production,” *Pediatr Neurosurg*, vol. 36, no. 1, pp. 22–28, 2002, doi: 10.1159/000048344.

[27] L. Xie *et al.*, “Sleep Drives Metabolite Clearance from the Adult Brain,” *Science*, vol. 342, no. 6156, pp. 373–377, Oct. 2013, doi: 10.1126/SCIENCE.1241224.

[28] Y. Aihara, T. Kawamata, T. Mitsuyama, T. Hori, and Y. Okada, “Novel method for controlling cerebrospinal fluid flow and intracranial pressure by use of a tandem shunt valve system,” *Pediatr Neurosurg*, vol. 46, no. 1, pp. 12–18, Jun. 2010, doi: 10.1159/000314052.

[29] J. D. Pickard and M. Czosnyka, “Management of raised intracranial pressure,” *J Neurol Neurosurg Psychiatry*, vol. 56, no. 8, pp. 845–858, 1993, doi: 10.1136/JNNP.56.8.845.

[30] J. Sotelo, “The hydrokinetic parameters of shunts for hydrocephalus might be inadequate,” *Surg Neurol Int*, vol. 3, no. 1, Jan. 2012, doi: 10.4103/2152-7806.94292.

[31] “Hydrocephalus | National Institute of Neurological Disorders and Stroke.” Accessed: Oct. 20, 2023. [Online]. Available: https://www.ninds.nih.gov/health-information/disorders/hydrocephalus

[32] “What is Hydrocephalus? | Hydrocephalus Association.” Accessed: Oct. 20, 2023. [Online]. Available: https://www.hydroassoc.org/about-hydrocephalus/

[33] “Common Cause of Acquired Hydrocephalus.” Accessed: Oct. 20, 2023. [Online]. Available: https://www.hydroassoc.org/acquired-hydrocephalus/

[34] A. P. Huang, L. T. Kuo, D. M. Lai, S. H. Yang, and M. F. Kuo, “Antisiphon device: A review of existing mechanisms and clinical applications to prevent overdrainage in shunted hydrocephalic patients,” *Biomed J*, vol. 45, no. 1, pp. 95–108, Feb. 2022, doi: 10.1016/J.BJ.2021.08.001.

[35] Y. Kajimoto *et al.*, “Posture-related changes in the pressure environment of the ventriculoperitoneal shunt system,” *J Neurosurg*, vol. 93, no. 4, pp. 614–617, Oct. 2000, doi: 10.3171/JNS.2000.93.4.0614.

[36] J. Ekstedt, “CSF hydrodynamic studies in man. 2 . Normal hydrodynamic variables related to CSF pressure and flow,” *J Neurol Neurosurg Psychiatry*, vol. 41, no. 4, pp. 345–353, 1978, doi: 10.1136/JNNP.41.4.345.

[37] “Developed high torque stepper motors in the world’s smallest size ! | FDK.” Accessed: Oct. 22, 2023. [Online]. Available: https://www.fdk.com/whatsnew-e/release0610021-e.html